Journal of Ophthalmology

Multimodal Imaging of the Fundus

Guest Editors: Atsushi Hayashi, Osman Cekic, Masanori Hangai, Yoshinori Mitamura, and Andreas W. A. Weinberger

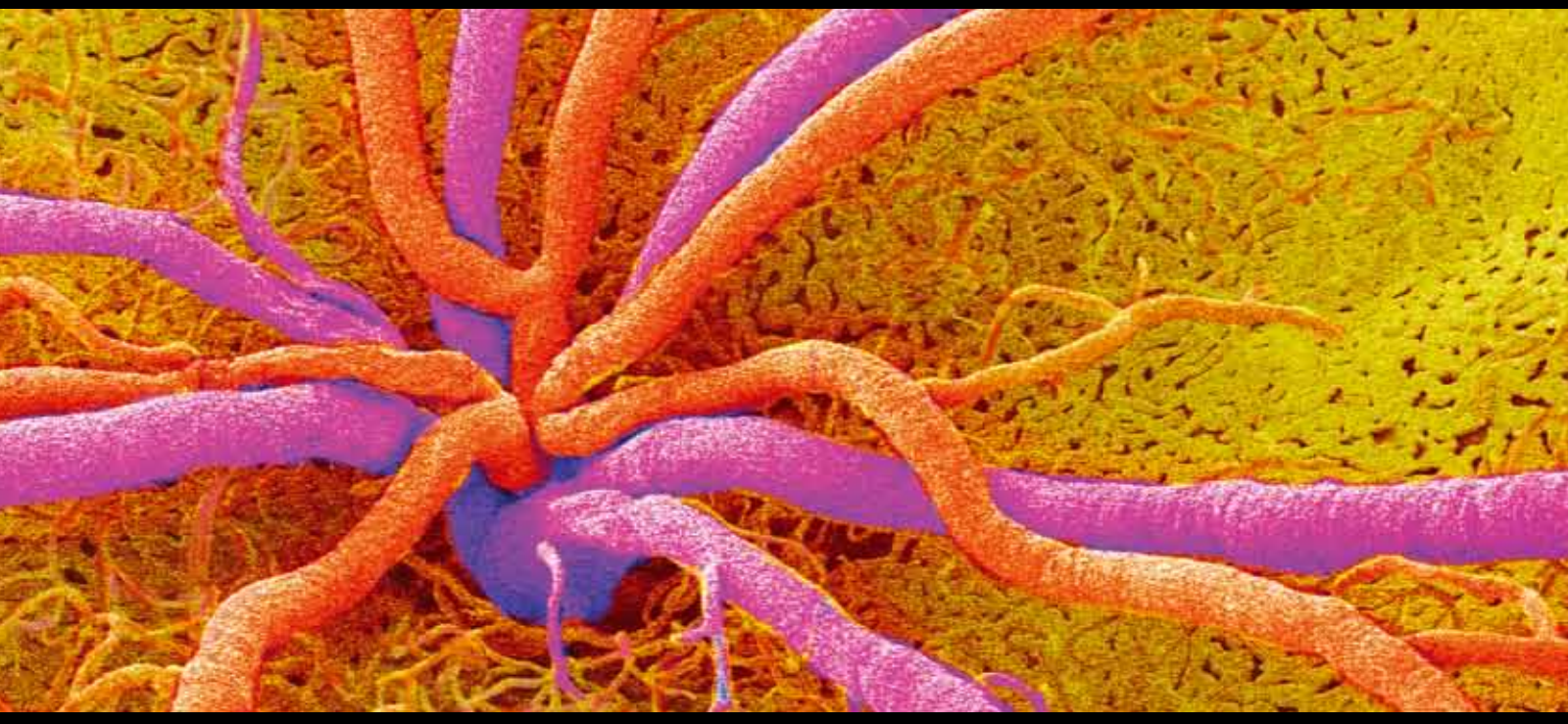

Multimodal Imaging of the Fundus

Journal of Ophthalmology

Multimodal Imaging of the Fundus

Guest Editors: Atsushi Hayashi, Osman Cekic, Masanori Hangai, Yoshinori Mitamura, and Andreas W. A. Weinberger

Editorial Board

Contents

Hindawi Publishing Corporation
Journal of Ophthalmology
Volume 2013, Article ID 956761, 1 page
http://dx.doi.org/10.1155/2013/956761

Editorial

Multimodal Imaging of the Fundus

Atsushi Hayashi,[1] Osman Cekic,[2] Masanori Hangai,[3] Yoshinori Mitamura,[4] and Andreas W. A. Weinberger[5]

[1] *Department of Ophthalmology, Graduate School of Medicine and Pharmaceutical Sciences, University of Toyama, Toyama 930-0194, Japan*
[2] *Department of Ophthalmology, Marmara University School of Medicine, 34903 Istanbul, Turkey*
[3] *Department of Ophthalmology, Kurume University School of Medicine, Fukuoka 830-0011, Japan*
[4] *Department of Ophthalmology, Institute of Health Biosciences, University of Tokushima Graduate School, Tokushima 770-8503, Japan*
[5] *Department of Ophthalmology, RWTH Aachen University, 52074 Aachen, Germany*

Correspondence should be addressed to Atsushi Hayashi; ahayashi@med.u-toyama.ac.jp

Received 12 June 2013; Accepted 12 June 2013

Retinal imaging devices made dramatic progress in these several years. These new devices reveal various anatomical and functional changes in the fundus by high resolution images, which may develop and improve diagnosis, treatment, and surgical maneuver.

The special issue on multimodal imaging of the fundus published one review article and five clinical research articles. The review article of Y. Mitamura et al. showed that the three lines in the outer retina detected by spectral-domain optical coherence tomography (SD-OCT) could serve as hallmarks for evaluation of photoreceptor condition in retinitis pigmentosa and recovery process after macular hole surgery. Of the five clinical research articles, N. F. Mokwa et al. compared sensitivity and specificity of imaging techniques of color fundus photography, fluorescein angiography, and SD-OCT for detecting age-related macular degeneration (AMD) and activity of choroidal neovascularization (CNV). F. Pichi et al. evaluated multimodal visualization of retinal genetic diseases by fundus autofluorescence, FA, indocyanine green (ICG) angiography, and SD-OCT to monitor progression of the diseases. O. A. Osmanbasoglu et al. analyzed diurnal variation of central choroidal thickness by enhanced depth imaging technique of SD-OCT in healthy emmetropic subjects. M. Şahin et al. reported hyperautofluorescence after cataract surgery, and J. M. Muñoz et al. compared ranges of contrast values in autofluorescence imaging between 2 fundus cameras.

All the six articles in this special issue underwent a rigorous peer-review process.

Acknowledgment

We are thankful to the referees for this work to meet the quality requirements of the accepted papers to ensure that it conforms to the standards of this journal. We sincerely hope that the readers will find the articles of interest and obtain useful information to understand clinical applications of multimodal imaging of the fundus.

Atsushi Hayashi
Osman Cekic
Masanori Hangai
Yoshinori Mitamura
Andreas W. A. Weinberger

Hindawi Publishing Corporation
Journal of Ophthalmology
Volume 2013, Article ID 385915, 6 pages
http://dx.doi.org/10.1155/2013/385915

Clinical Study

Grading of Age-Related Macular Degeneration: Comparison between Color Fundus Photography, Fluorescein Angiography, and Spectral Domain Optical Coherence Tomography

Nils F. Mokwa,[1] Tina Ristau,[1] Pearse A. Keane,[2] Bernd Kirchhof,[1] Srinivas R. Sadda,[3] and Sandra Liakopoulos[1]

[1] *Cologne Image Reading Center and Laboratory, Department of Ophthalmology, University of Cologne, 50924 Cologne, Germany*
[2] *Biomedical Research Centre for Ophthalmology, Moorfields Eye Hospital NHS Foundation Trust and UCL Institute of Ophthalmology, London EC1V 2PD, UK*
[3] *Doheny Image Reading Center, Doheny Eye Institute, Keck School of Medicine of the University of Southern California, Los Angeles, CA 90033, USA*

Correspondence should be addressed to Sandra Liakopoulos; sandra.liakopoulos@uk-koeln.de

Received 18 January 2013; Accepted 8 April 2013

Academic Editor: Andreas W. A. Weinberger

Purpose. To compare color fundus photography (FP), fluorescein angiography (FA), and spectral domain optical coherence tomography (SDOCT) for the detection of age-related macular degeneration (AMD), choroidal neovascularisation (CNV), and CNV activity. *Methods*. FPs, FAs, and SDOCT volume scans from 120 eyes of 66 AMD and control patients were randomly collected. Control eyes were required to show no AMD, but other retinal pathology was allowed. The presence of drusen, pigmentary changes, CNV, and signs for CNV activity was independently analyzed for all imaging modalities. *Results*. AMD was diagnosed based on FP in 75 eyes. SDOCT and FA showed sensitivity (specificity) of 89% (76%) and 92% (82%), respectively. CNV was present on FA in 68 eyes. Sensitivity (specificity) was 78% (100%) for FP and 94% (98%) for SDOCT. CNV activity was detected by SDOCT or FA in 60 eyes with an agreement in 46 eyes. Sensitivity was 88% for SDOCT and 88% for FA. FP showed sensitivity of 38% and specificity of 98%. *Conclusions*. CNV lesions and activity may be missed by FP alone, but FP may help identifying drusen and pigmentary changes. SDOCT is highly sensitive for the detection of AMD, CNV, and CNV activity; however, it cannot fully replace FA.

1. Introduction

Prior to the antivascular endothelial growth factor (anti-VEGF) era, age-related macular degeneration (AMD) was considered the leading cause of severe visual loss and blindness in the developed world among people over the age of 50 years [1]. Various imaging methods are available for the diagnosis and classification of AMD. Until recently, color fundus photography (FP) was the gold standard for grading and staging in AMD clinical trials [2–4]. By permitting visualisation of the choroidal and retinal microcirculation and providing detailed information about the presence of pathological vessels as well as the integrity of the blood retinal barrier, fluorescein angiography (FA) had become a central tool for detecting and classifying CNV as well as CNV activity in eyes with neovascular AMD [5, 6].

During the past years, OCT has dramatically gained importance for the diagnosis and management of patients with chorioretinal disease by noninvasively providing cross-sectional images of the neurosensory retina and the subretinal space, thus allowing a detailed characterization of structural changes. Thus, OCT is increasingly used to determine the presence and activity of CNV and the need for (re-) treatment [7–9]. New-generation spectral domain OCT (SDOCT) instruments provide even higher resolution and more dense coverage of the macular area compared with time

Table 1: Parameters evaluated as signs for AMD, CNV, and CNV activity.

	Color fundus photography	Fluorescein angiography	SDOCT
AMD	Presence of ≥10 small hard drusen and pigmentary changes or ≥1 intermediate or large drusen inside the 6 mm ETDRS grid		
CNV	Fibrosis, fibrovascular tissue, or fibrin either subretinal or subRPE (not related to any other retinal vascular disease but CNV)	Classic or occult CNV or staining scar	Subretinal hyperreflective material or PED other than single drusen
CNV activity	Fluid or hemorrhage related to CNV	Classic or occult CNV leakage	Diffuse or cystoid intraretinal fluid or subretinal fluid

AMD: age-related macular degeneration; CNV: choroidal neovascularization; FA: fluorescein angiography; SDOCT: spectral-domain optical coherence tomography; RPE: retinal pigment epithelium; and PED: pigment epithelial detachment.

domain OCT [10]. Therefore, SDOCT imaging is now widely used for the followup of patients with CNV undergoing anti-VEGF therapy.

This study aims to compare FP, FA, and SDOCT imaging regarding their sensitivity and specificity for detecting AMD, CNV, and CNV activity and to analyze whether SDOCT may have the potential to replace the other imaging techniques.

2. Materials and Methods

2.1. Data Collection. The European Genetic Database (EUGENDA), a database collecting AMD patients as well as healthy controls, was retrospectively reviewed, and FP, FA, and SDOCT images of 120 eyes of 66 consecutive patients were randomly collected. Eyes with early, intermediate, or late AMD as well as control cases were included. Control eyes were required to show no signs for AMD, but other chorioretinal diseases including CNV secondary to any other disease but AMD was allowed. To be eligible for this study, all images had to be performed on the same day at the University of Cologne, Germany.

FPs were performed using the Canon 60 UVi fundus camera. For all patients, one 40° stereo pair centred on the fovea was captured. FA images were performed using the Spectralis HRA system (Heidelberg Engineering, Heidelberg, Germany). The standard protocol included 30° stereo images of the transit phase, mid phase, and late phase up to 10 minutes following intravenous injection of fluorescein. SDOCT images were acquired using the Spectralis SDOCT instrument (Heidelberg Engineering, Heidelberg, Germany). SDOCT volume scans (15° × 20°) composing of 37 parallel OCT B-scans were used for analysis. For each OCT B-scan, 20 images were averaged using the automated real-time (ART) function.

2.2. Image Analysis. Images were independently analyzed by reading center graders (TR, NFM, and SL) at the Cologne Image Reading Center (CIRCL), which have been trained and certified in image interpretation of AMD patients. Discrepancies between graders have been solved by open adjudication.

During analysis of one imaging technique, the grader was masked to all other images and grading results of the patient. For all images, the presence of AMD, CNV, and CNV activity was noted (Table 1, Figure 1).

AMD was defined as the presence of ≥10 small (≤63 μm), hard drusen and pigmentary changes or at least 1 intermediate (64–124 μm) or large (≥125 μm) drusen inside the 6 mm ETDRS grid.

CNV was considered present on FP, if subretinal or subRPE fibrosis and fibrovascular tissue or fibrin were seen; on SDOCT, subretinal hyperreflective material or pigment epithelial detachments (PEDs) other than single drusen were considered signs for CNV. On FA, CNV lesions were graded according to the modified Macular Photocoagulation Study (MPS) grading protocol utilized in the treatment of AMD with photodynamic therapy (TAP) and verteporfin in photodynamic therapy (VIP) studies [11, 12]. Briefly, classic CNV was identified as an area of uniform early hyperfluorescence that showed extensive leakage in the mid and late phases. Occult CNV was classified as areas of stippled hyperfluorescence that appeared in the mid and late phases of the fluorescein angiography. CNV was graded as present on FA, if classic or occult CNV lesion components or staining scar tissue was detected.

CNV activity was noted, if fluid or hemorrhage was present on FP that was not related to any other retinal vascular disease but CNV, if classic or occult CNV leakage was detected on FA or if diffuse or cystoid intraretinal fluid or subretinal fluid accumulation was seen on SDOCT.

2.3. Statistical Methods. For each parameter to be evaluated, the following imaging modalities were defined as the gold standard: for presence of AMD, FP was used as the gold standard. For the presence of CNV, FA was defined as the gold standard. CNV activity was considered present if it was detected on either SDOCT or FA (ground truth). Sensitivity and specificity values for each imaging modality were calculated against the gold standard. This study adhered to the tenets set forth in the Declaration of Helsinki.

3. Results

A summary of grading results is provided in Table 2.

Seventy-five eyes were diagnosed with AMD based on FP. Signs for AMD were detected on FA in 77 eyes with a sensitivity of 92% (69 out of 75) and a specificity of 82% (in 8 cases, AMD was noted on FA but not on color fundus photographs). Disagreement between FA and FP was mainly related to small drusen that have been noted on FA but not on FP, and RPE hyperpigmentation that has been seen on FPs but not on FAs. On SDOCT, AMD was considered present

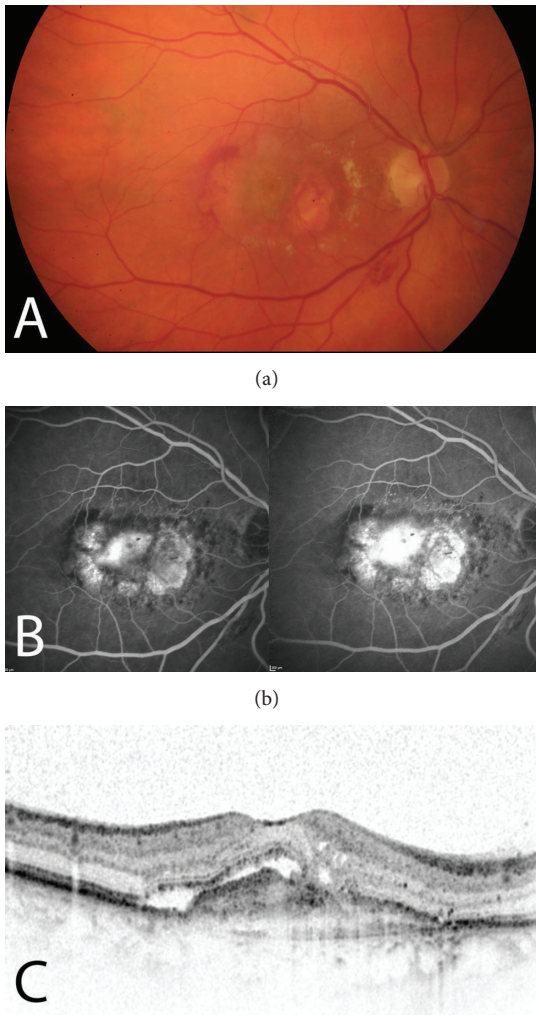

Figure 1: Eye with active CNV. Color fundus photography (a) demonstrates hemorrhage and fibrovascular tissue, fluorescein angiography (b) shows classic and occult CNV leakage, and SDOCT (c) presents intraretinal cystoid spaces, subretinal fluid, subretinal hyperreflective material, and a pigment epithelial detachment.

in 78 eyes with a sensitivity of 89% (67 out of 75) and a specificity of 76% (in 11 cases, signs for AMD were noted on SDOCT but not on FP). Disagreement between SDOCT and FP could mainly be explained by small or intermediate drusen and RPE changes that have been missed on SDOCT and by intermediate drusen that have been noted on SDOCT but not on FPs.

Forty-five eyes were included in the control group.Twenty out of those eyes showed pathologies other than AMD, including high myopia, chorioretinitis, retinal vein occlusion, epiretinal membranes, diabetic retinopathy and central serous retinopathy, or idiopathic CNV. CNV was diagnosed in 68 eyes using FA as the gold standard. Fifty-four out of those cases were diagnosed with AMD based on FPs. In 14 cases, CNV was seen in the control group (idiopathic or related to high myopia or chorioretinitis). FP showed a sensitivity of 78% (53 out of 68 eyes) for the detection of CNV, and a specificity of 100%. SDOCT images showed signs for CNV in 64 out of the 68 cases (94%), specificity for detecting CNV was 98% (in one case, CNV was diagnosed based on SDOCT but not on FA). In the 64 cases with agreement between FA and SDOCT regarding the presence of CNV, a classic CNV lesion component was detected on FA in 25 eyes. SDOCT revealed subretinal hyperreflective material in all of these cases. Additionally, subretinal hyperreflective material was seen in 15 eyes without classic CNV leakage. Ten out of those 15 cases showed staining scar as a lesion component on FA, and 5 cases demonstrated occult CNV leakage only. Thirty-eight out of the 64 cases showed occult CNV lesion components on FA, with all of those demonstrating a PED on SDOCT. In addition, a PED was seen in 22 eyes without occult CNV lesion components on FA, with 18 (82%) out of those cases demonstrating staining scar as a lesion component and 4 (18%) cases showing classic CNV leakage only.

Out of the 68 cases with CNV diagnosed based on FA, a total of 60 cases (88%) showed signs for active CNV either on SDOCT (53 eyes) or FA (53 eyes), with an agreement between both imaging modalities in 79% out of all 68 cases (46 cases showed active CNV and 8 eyes no signs for CNV activity on both imaging modalities). In 7 cases, fluid was detected on SDOCT without evidence for CNV leakage on FA and vice versa. If the ground truth for SDOCT and FA was considered the gold standard for CNV activity, sensitivity was 88% for FA, 88% for SDOCT, and 38% (23 out of 60) for FP, respectively. Specificity for FP was 98% (in one case, CNV activity was suspected based on FP but not seen on FA or SDOCT).

4. Discussion

SDOCT is increasingly used in clinical trials as well as in clinical practice for the diagnosis and followup of patients with neovascular AMD undergoing anti-VEGF therapy [13]. As a noninvasive imaging tool, it provides high-resolution cross-sectional images of retinal pathology, allowing to qualitatively and quantitatively analyze various parameters relevant for (re-) treatment decisions. Our study confirms that SDOCT is highly sensitive for detecting AMD, CNV, and CNV activity; however, it may not yet fully replace the information provided by FA and FP.

The presence of characteristic features of AMD on FP such as drusen and RPE changes was missed on SDOCT in 11% of cases in our study. This may be explained by the SDOCT volume scan settings used, as the gap between two parallel OCT B-scans was approximately 120 μm; thus pathological changes may fall in between two adjacent scans and may be overlooked or may appear smaller than they truly are. On the other hand, AMD was diagnosed on SDOCT based on the presence of intermediate drusen in 24% of cases that were graded as control cases on FP. On FP, those pathological features have been either interpreted as RPE changes or small drusen, or they have been overlooked due to reduced image clarity. Thus, SDOCT may be helpful in identifying drusen and in differentiating drusen from hypopigmentation and

Table 2: Sensitivity and specificity in detecting AMD, CNV, and CNV activity.

	Color fundus photography	Fluorescein angiography	SDOCT
AMD *n* (sensitivity/specificity)	75 (gold standard)	77 (92%/82%)	78 (89%/76%)
CNV *n* (sensitivity/specificity)	53 (78%/100%)	68 (gold standard)	69 (94%/98%)
CNV activity *n* (sensitivity/specificity)	24 (38%/98%)	Ground truth used as gold standard ($n = 60$)	
		53 (sensitivity 88%)	53 (sensitivity 88%)

AMD: age-related macular degeneration; CNV: choroidal neovascularization; and SDOCT: spectral-domain optical coherence tomography.

thus may improve the quality of image interpretation in eyes with AMD compared to FP imaging alone. However, care should be taken not to transfer size definitions for intermediate or large drusen from FPs to SDOCT, as due to their shape, drusen may appear larger on SDOCT compared to FP, or they may appear smaller if they are captured at the border [14]. Further studies are needed to compare drusen sizes between those different imaging modalities before SDOCT imaging can be reliably used for staging of early and intermediate AMD in clinical trials. Other imaging techniques such as autofluorescence imaging provide additional information concerning drusen and RPE changes and may thus be helpful to identify and classify those features.

FA is commonly used as the gold standard for evaluating CNV lesions. Based on FA, CNV lesions components are categorized as classic or occult CNV leakage or staining scar tissue that may develop over time and indicate longstanding disease with poor visual function [11]. SDOCT appeared to be highly sensitive and specific in detecting CNV in our study. Do et al. reported a sensitivity of only 40% for the detection of new-onset CNV on time-domain OCT [15]. The low sensitivity may be explained by the use of time-domain OCT, as pathological features may be overlooked more easily compared to SDOCT due to the less dense scan pattern, lower image resolution, and higher rate of movement artifacts [10].

Occult CNV on FA is believed to correspond histologically to type 1 CNV, located between the RPE and Bruch's membrane [16]. In accordance with this, all eyes with occult CNV on FA demonstrated a PED on SDOCT in our study. In contrast, classic CNV lesion components on FA histologically correspond to type 2 CNV, positioned in the subretinal space [16]. Thus, type 2 CNV lesion components are expected to present as hyperreflective material in the subretinal space on OCT. This could be confirmed in our study as all cases with classic CNV lesion components on FA demonstrated subretinal hyperreflective material on SDOCT. However, in order to correctly interpret OCT images, it is crucial to consider that OCT scans only represent "pseudohistological" images, created using information about the reflectivity and axial distribution of various structures. Hence, subretinal hyperreflective material on OCT scans may not only represent type 2 CNV, but may include, for example, subretinal hemorrhage, fibrinous material, or photoreceptor debris. This may explain why subretinal hyperreflective material was seen in our study on SDOCT in 5 cases demonstrating occult CNV on FA without the presence of a classic CNV leakage or staining scar as lesion components.

Additionally, a PED was seen on SDOCT in 22 eyes without the presence of occult CNV on FA. In those cases, other CNV lesion components such as staining scar or classic CNV may have covered the CNV membrane located in the sub-RPE space; thus occult CNV leakage was not detectable on FA. This finding indicates that high-resolution cross-sectional images provided by SDOCT may add important information regarding subretinal and sub-RPE pathology compared to the two-dimensional en-face view of FA and FP imaging.

Agreement between SDOCT and FA regarding the activity of CNV lesions in our study was seen in 79% of all 68 cases diagnosed with CNV on FA. Seven eyes demonstrated CNV leakage on FA in the absence of intra- or subretinal fluid on SDOCT, and 7 eyes showed signs for CNV activity on SDOCT without evidence of CNV leakage on FA. This discrepancy was also described in other reports [17–19]. Khurana et al. reported a sensitivity of 90% and specificity of 47% for SDOCT to detect CNV activity seen on FA [17].

The disagreement between both imaging modalities may be explained by the fact that FA and SDOCT imaging provides different information about retinal pathology. FA is used to obtain information about the perfusion and the growth of new vessels as well as the integrity of the blood-retinal barrier; thus fluorescein leakage over time can be seen during angiography. This information is missing on OCT images; thus OCT provides detailed information about pathological changes like, for example, the presence of cystoid spaces; however, it is not possible to detect whether they are caused by fluid accumulation from acute leakage from pathological vessels. Thus, cystoid spaces on SDOCT may not necessarily correspond to fluorescein leakage on FA, but may represent structural defects indicating chronic disease (Figure 2). Increase or decrease in the amount of fluid seen on OCT may thus more reliably indicate CNV activity than the presence of fluid seen at one time point. In addition, care should be taken to not confuse intraretinal cystoid spaces or subretinal fluid with "outer retinal tubulations," a SDOCT finding described by Zweifel et al. [20]. In their paper, the authors state that degenerating photoreceptors may become arranged in a circular or ovoid fashion in chronic diseases affecting the outer retina and RPE.

In contrast, CNV activity seen on FA may be missed on SDOCT if only intraretinal cystoid spaces and subretinal fluid accumulation are considered to represent CNV activity on SDOCT. Giani et al. recently reported that intraretinal hyperreflective flecks and the inherent reflectivity and boundary

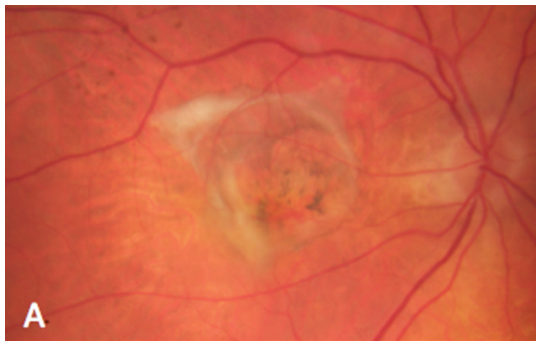

(a)

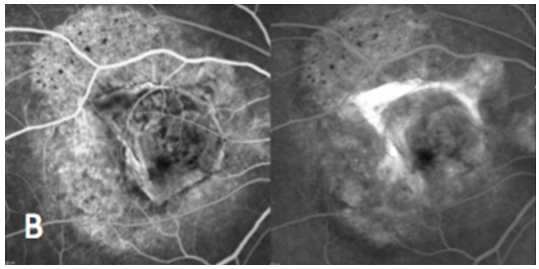

(b)

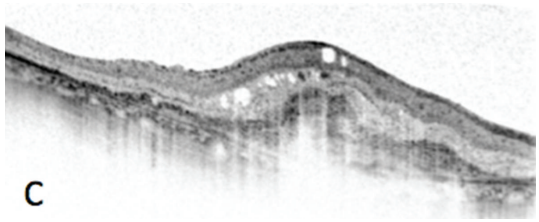

(c)

Figure 2: Discrepancy between imaging modalities regarding identification of signs considered to indicate CNV activity: color fundus photography (a) demonstrates fibrosis and RPE changes, fluorescein angiography (b) demonstrates staining of CNV, and SDOCT (c) shows intraretinal cystoid spaces.

definition of subretinal hyperreflective material may indicate active CNV even in the absence of intra- or subretinal fluid accumulation [21]. Additionally, fluid accumulation in the sub-RPE space such as serous components of a PED may indicate CNV activity.

FA imaging at baseline in addition to SDOCT is helpful to assess the CNV lesion subtype and the initial severity of CNV leakage; during followup, FA may confirm evidence of CNV activity whenever SDOCT interpretation is challenging or inconsistent with retinal function.

5. Conclusions

SDOCT, FA, and FP imaging provide complementary information about pathological changes in chorioretinal diseases. Our study indicates that drusen and RPE changes as signs for AMD are best appreciated on FP. SDOCT is highly sensitive to identify CNV and CNV activity; however, it cannot fully replace FA in the management of patients with CNV. Further studies are needed to evaluate which SDOCT parameters (e.g., cystoid spaces, diffuse intraretinal fluid, subretinal or sub-RPE fluid, inherent boundary definition of subretinal hyperreflective material, or a change in the amount of fluid) best indicate CNV activity.

Financial Disclosure

Srinivas R. Sadda is a coinventor of Doheny intellectual property related to optical coherence tomography that has been licensed by Topcon Medical Systems and a member of the scientific advisory board for Heidelberg Engineering. Srinivas R. Sadda also receives research support from Carl Zeiss Meditec, Optos, and Optovue, Inc. However, it is not related to the subject matter of this paper.

Acknowledgment

This research has been supported in part by the Retinovit Foundation, Cologne, Germany.

References

[1] N. M. Bressler, "Age-related macular degeneration is the leading cause of blindness," *Journal of the American Medical Association*, vol. 291, no. 15, pp. 1900–1901, 2004.

[2] A. C. Bird, N. M. Bressler, S. B. Bressler et al., "An international classification and grading system for age-related maculopathy and age-related macular degeneration: the International ARM Epidemiological Study group," *Survey of Ophthalmology*, vol. 39, no. 5, pp. 367–374, 1995.

[3] Age-Related Eye Disease Study Research Group, "The Age-Related Eye Disease Study system for classifying age-related macular degeneration from stereoscopic color fundus photographs: the Age-Related Eye Disease Study Report Number 6," *American Journal of Ophthalmology*, vol. 132, no. 5, pp. 668–681, 2001.

[4] J. M. Seddon, S. Sharma, and R. A. Adelman, "Evaluation of the clinical age-related maculopathy staging system," *Ophthalmology*, vol. 113, no. 2, pp. 260–266, 2006.

[5] P. J. Rosenfeld, D. M. Brown, J. S. Heier et al., "Ranibizumab for neovascular age-related macular degeneration," *The New England Journal of Medicine*, vol. 355, no. 14, pp. 1419–1431, 2006.

[6] D. M. Brown, P. K. Kaiser, M. Michels et al., "Ranibizumab versus verteporfin for neovascular age-related macular degeneration," *The New England Journal of Medicine*, vol. 355, no. 14, pp. 1432–1444, 2006.

[7] P. K. Kaiser, B. A. Blodi, H. Shapiro, and N. R. Acharya, "Angiographic and optical coherence tomographic results of the MARINA study of ranibizumab in neovascular age-related macular degeneration," *Ophthalmology*, vol. 114, no. 10, pp. 1868–e4, 2007.

[8] A. E. Fung, G. A. Lalwani, P. J. Rosenfeld et al., "An optical coherence tomography-guided, variable dosing regimen with intravitreal ranibizumab (Lucentis) for neovascular age-related macular degeneration," *American Journal of Ophthalmology*, vol. 143, no. 4, pp. 566–583, 2007.

[9] D. F. Martin, M. G. Maguire, G. S. Ying, J. E. Grunwald, S. L. Fine, and G. J. Jaffe, "Ranibizumab and bevacizumab for neovascular age-related macular degeneration. CATT Research

Group," *The New England Journal of Medicine*, vol. 364, no. 20, pp. 1897–1908, 2011.

[10] P. A. Keane, R. A. Bhatti, J. W. Brubaker, S. Liakopoulos, S. R. Sadda, and A. C. Walsh, "Comparison of clinically relevant findings from high-speed fourier-domain and conventional time-domain optical coherence tomography," *American Journal of Ophthalmology*, vol. 148, no. 2, pp. 242–248, 2009.

[11] I. Barbazetto, A. Burdan, N. M. Bressler et al., "Photodynamic therapy of subfoveal choroidal neovascularization with verteporfin: fluorescein angiographic guidelines for evaluation and treatment—TAP and VIP report no. 2," *Archives of Ophthalmology*, vol. 121, no. 9, pp. 1253–1268, 2003.

[12] B. S. Hawkins and S. L. Fine, "Laser photocoagulation of subfoveal neovascular lesions of age-related macular degeneration: updated findings from two clinical trials," *Archives of Ophthalmology*, vol. 111, no. 9, pp. 1200–1209, 1993.

[13] P. A. Keane, P. J. Patel, S. Liakopoulos, F. M. Heussen, S. R. Sadda, and A. Tufail, "Evaluation of age-related macular degeneration with optical coherence tomography," *Survey of Ophthalmology*, vol. 57, no. 5, pp. 389–414, 2012.

[14] N. Jain, S. Farsiu, A. A. Khanifar et al., "Quantitative comparison of drusen segmented on SD-OCT versus drusen delineated on color fundus photographs," *Investigative Ophthalmology and Visual Science*, vol. 51, no. 10, pp. 4875–4883, 2010.

[15] D. V. Do, E. W. Gower, S. D. Cassard et al., "Detection of new-onset choroidal neovascularization using optical coherence tomography: the AMD DOC study," *Ophthalmology*, vol. 119, no. 4, pp. 771–778, 2012.

[16] H. E. Grossniklaus and J. D. M. Gass, "Clinicopathologic correlations of surgically excised type 1 and type 2 submacular choroidal neovascular membranes," *American Journal of Ophthalmology*, vol. 126, no. 1, pp. 59–69, 1998.

[17] R. N. Khurana, B. Dupas, and N. M. Bressler, "Agreement of time-domain and spectral-domain optical coherence tomography with fluorescein leakage from choroidal neovascularization," *Ophthalmology*, vol. 117, no. 7, pp. 1376–1380, 2010.

[18] N. Eter and R. F. Spaide, "Comparison of fluorescein angiography and optical coherence tomography for patients with choroidal neovascularization after photodynamic therapy," *Retina*, vol. 25, no. 6, pp. 691–696, 2005.

[19] I. Kozak, V. L. Morrison, T. M. Clark et al., "Discrepancy between fluorescein angiography and optical coherence tomography in detection of macular disease," *Retina*, vol. 28, no. 4, pp. 538–544, 2008.

[20] S. A. Zweifel, M. Engelbert, K. Laud, R. Margolis, R. F. Spaide, and K. B. Freund, "Outer retinal tubulation a novel optical coherence tomography finding," *Archives of Ophthalmology*, vol. 127, no. 12, pp. 1596–1602, 2009.

[21] A. Giani, C. Luiselli, D. D. Esmaili et al., "Spectral-domain optical coherence tomography as an indicator of fluorescein angiography leakage from choroidal neovascularization," *Investigative Ophthalmology & Visual Science*, vol. 52, no. 8, pp. 5579–5586, 2011.

Hindawi Publishing Corporation
Journal of Ophthalmology
Volume 2013, Article ID 376013, 5 pages
http://dx.doi.org/10.1155/2013/376013

Clinical Study

Evaluation of Cystoid Macular Edema Using Optical Coherence Tomography and Fundus Autofluorescence after Uncomplicated Phacoemulsification Surgery

Muhammed Şahin,[1] Abdullah Kürşat Cingü,[1] and Nilüfer Gözüm[2]

[1] *Department of Ophthalmology, Faculty of Medicine, Dicle University, 21280 Diyarbakir, Turkey*
[2] *Department of Ophthalmology, Faculty of Medicine, Istanbul University, 34093 Istanbul, Turkey*

Correspondence should be addressed to Muhammed Şahin; drmuhammedsahin@gmail.com

Received 24 January 2013; Revised 8 April 2013; Accepted 9 April 2013

Academic Editor: Atsushi Hayashi

Aim. To investigate the utility of fundus autofluorescence (FAF) and optical coherence tomography (OCT) in the evaluation of cystoid macular edema (CME) following cataract surgery. *Materials and Methods*. Forty eyes of 29 patients undergone phacoemulsification, with posterior chamber intraocular lens implantation surgery. Central macular thickness (CMT) of the patients was evaluated using OCT and FAF preoperatively and postoperative 1st, 30th, 60th, 90th, and 180th days. *Results*. CME was detected in three eyes (7.5%) of two patients using OCT. Hyperautofluorescence (HAF) was detected in two of these three eyes and resolved with treatment. In the remaining 37 eyes without CME, there was a significant increase in visual acuity when compared to preoperative values ($P = 0.008$) Mean macular thicknesses (MMT) of the eyes without CME were $174 \pm 20\,\mu$m preoperatively and $179 \pm 22\,\mu$m at day 1, $178 \pm 19\,\mu$m at 1st month, and $168 \pm 10\,\mu$m at 6th month postoperatively. In the eyes with CME, the MMTs, measured with OCT were $189 \pm 23\,\mu$m preoperatively and 432 ± 361 on day 1, $343 \pm 123\,\mu$m at 1st month, 345 ± 196 at 2nd month, and $200 \pm 36\,\mu$m at 6th month postoperatively. *Conclusion*. We found a moderate increase in CMT in the first 3 months postoperatively, in the eyes without CME which did not cause visual disturbances. FAF is a noninvasive, rapid method for the evaluation and follow-up of CME following cataract surgery.

1. Introduction

Cystoid macular edema (CME) is the formation of fluid-filled cystoid spaces between the outer plexiform and inner nuclear layers of the retina, resulting from disruption of the blood-retinal barrier. It is a common complication observed after cataract surgery, with or without other complications. The rate of CME increases in the presence of diabetic retinopathy and uveitis. Although the pathogenesis is still not fully understood, the diagnosis is usually easily confirmed by clinical or angiographic examinations. With modern surgical techniques the incidence of CME has decreased to 1% [1, 2].

The incidence of angiographic CME, without clinical macular edema, has been reported to be around 10–20% following cataract surgery. While it usually occurs 4–12 weeks following surgery; there are a few cases reported after many months or years after the surgery [3].

Optical coherence tomography (OCT) is a noninvasive and quantitative imaging modality, which provides cross-sectional images of the retina, with the help of ~800 nm diode laser light [4–7]. OCT has become an important diagnostic method, especially in retinal diseases, such as CME, diabetic macular oedema, macular hole, and glaucoma.

Autofluorescence (AF) can be defined as light scatter from the structures in the eye, without the use of fluorescein dye. Fundus autofluorescence (FAF) arises from lipofuscin in the retinal pigment epithelium (RPE) cells [8]. Hyper-autofluorescence (HAF) in CME occurs as a result of the displacement of macular pigments into the cystoid gaps. HAF also occurs when inflammation triggers the pro-oxidative pathway. Blue light with a wavelength of 488 nm is used for FAF imaging using Heidelberg Retinal Angiography (HRA) or a modified fundus camera [9, 10].

Table 1: The mean preoperative and postoperative best corrected visual acuity and the mean central macular thickness measurements of patients.

Features	Time of intervention	CME (−) group SD ($n = 37$)	CME (+) group SD ($n = 3$)
BCVA (Snellen)	Preop	0.43 (0.21)	0.40 (0.14)
	Postop 1st day	0.51 (0.26)	0.21 (0.14)
	Postop 1st mo	0.84 (0.21)	0.56 (0.23)
	Postop 2nd mo		0.70 (0.20)
	Postop 3rd mo	0.90 (0.15)	0.70 (0.20)
	Postop 6th mo	0.91 (0.14)	0.83 (0.05)
CMT	Preop	174 (20) μ	189 (23) μ
	Postop 1st day	179 (22) μ	432 (361) μ
	Postop 1st mo	178 (19) μ	343 (123) μ
	Postop 2nd mo		345 (196) μ
	Postop 3rd mo	172 (13) μ	219 (49) μ
	Postop 6th mo	168 (10) μ	200 (36) μ

CME: cystoid macular edema; SD: standard deviation; Preop: preoperative; BCVA: best corrected visual acuity; CMT: central macular thickness; Postop: postoperative; wk: week; mo: month; μ: mikron.

In the present study, we evaluated the central macular thickness (CMT) using noninvasive methods, including OCT and FAF, in patients who underwent cataract surgery without complication, using phacoemulsification (phaco) with posterior intraocular lens (PCIOL) implantation.

2. Materials and Methods

For this study, patients were selected from those who were diagnosed with juvenile or senile cataracts, who underwent phaco and PCIOL implantation with no complications, between October 2008 and June 2009 at the Department of Ophthalmology, Istanbul University, Istanbul Faculty of Medicine. Preoperatively, complete ophthalmologic examinations of the patients were performed, including uncorrected and best corrected visual acuities (BCVA), manifest refraction, keratometry, axial length, intraocular pressure, and biomicroscopic and posterior segment examinations. CMT of each eye was evaluated by a spectral domain-scanning laser ophthalmoscope OCT (SD-SLO/OCT) (OTI, Toronto, Canada). AF images were obtained using a HRA 1 device (Heidelberg Engineering, Germany), using the fluorescein mode without injection of fluorescein and using the red-free mode after the pupils were dilated and focused on the retina. The 30 micron visual field mode was used to obtain FAF images. A series of 20 images were recorded, digitalized, aligned, and averaged using image analysis using HRA 1 device. Patients with any ocular pathology, other than cataracts, were excluded from the study. The study was conducted in accordance with the tenets of the Declaration of Helsinki.

Cataract surgery was performed under local anesthesia, except for two patients whose operations were carried out under general anesthesia. Standard phaco procedures were performed on patients, with a 3 mm clear corneal incision and a foldable PCIOL implantation. Eyes that experienced any intraoperative complication were excluded from the study. Topical prednisolone sodium phosphate 1% (Norsol, Bilim İlaç, Turkey), six times daily, and topical tobramycin 0.3% (Tobrex, ALCON, USA), four times daily, were prescribed to the patients in the postoperative period. Postoperative examinations of the patients were performed on days 1, 30, 60, 90, and 180.

Patients were divided into two groups depending on the presence or absence of CME. An additional examination was performed for patients with CME at 2 months following the operation. Preoperative and postoperative values were recorded and compared between the two groups. Depending on clinical recovery, diclofenac sodium 75 mg tb (Voltaren SR, Novartis, USA), once daily, ketorolac tromethamine 0.5% (Acular, Allergan, Irvine, CA), four times daily, and topical prednisolone acetate 1% (Pred Forte, Allergan, Irvine, CA) were given to the patients with CME who showed no improvement in BCVA.

The findings of the study were analyzed using Statistical Package for Social Sciences (SPSS) for Windows 16.0. the Friedman nonparametric analysis of variance was performed for repeated measurements. The Wilcoxon test was used for comparisons in pairs by applying a Bonferroni correction. Pearson's correlation tests were used to determine the strength of the relationships between the measurements. Significance was evaluated at the level $P < 0.05$.

3. Results

Forty eyes of 29 patients were included in this study. Eleven of the 29 patients were male (37.9%), and 18 were female (62.1%). The mean age of the patients was 61.03 ± 16.72 years (range 10–79 years). The mean ages of the patients with CME and the patients without CME were 70.5 ± 10.6 and 60.33 ± 17.01, resepectively. Changes in visual acuity and CMT of patients are shown in Table 1. In the preoperative period, FAF and OCT images of the patients were normal. The foveal examination of the patients with slit lamp biomicroscopy, by using a +90 D noncontact lens, revealed CME in all eyes with the CMT approximately ≥200 μm. Postoperative BCVA did

Table 2: Statistical significance in the comparison of BVCA measurements without CME.

P values	Postop			
	1st day	1st mo	3rd mo	6th mo
Preop	0.26	0.001	0.001	0.008
1st day		0.001	0.001	0.008
1st mo			0.02	0.06
3rd mo				0.18

Preop: preoperative; Postop: postoperative; mo: month.

Table 3: Statistical significance in the comparison of OCT measurements without CME.

P values	Postop			
	1st day	1st mo	3rd mo	6th mo
Preop	0.03	0.63	0.93	0.79
1st day		0.43	0.24	0.17
1st mo			0.05	0.07
3rd mo				0.04

Preop: preoperative; Postop: postoperative; mo: month.

not increase in three of the eyes of two patients (7.5%), and CME was detected in these eyes by the use of OCT, FAF and during routine examination at 1 month.

A significant increase in the BCVA was observed in the eyes without CME after 1 month when compared to the examination at day 1 ($P = 0.001$) and at 3 months when compared to the examination at 1 month ($P = 0.02$), postoperatively (Table 2).

During the followup, there was a significant increase in CMT in the eyes without CME between the preoperative evaluation and day 1 postoperative ($P = 0.03$), at 1 month and 3 months ($P = 0.05$), and a significant decrease in CMT was seen at 6 months, when compared to the examination at 3 months ($P = 0.04$) (Table 3).

The CMT in patients without CME decreased to normal levels at 3 months. However, the preoperative values were lower than the postoperative values measured at 6 months which was not statistically significant. There was no significant correlation between BCVA and CMT in any of the postoperative examinations.

CME was detected in three of the eyes of two patients at 1 month, but HAF was observed only in two of these three eyes. The change in BCVA and the CMT and FAF and OCT images of these three patients are shown in Figure 1.

4. Discussion

CME is the most common cause of unexpected loss of vision after uncomplicated cataract surgery [11]. CME was first described by Irvine after intracapsular cataract extraction (ICCE) in 1953 [12]. In CME following cataract surgery, there are three mechanisms attributing to the etiology of CME: the effect of vitreoretinal traction, light damage, and production of prostaglandins. Development of clinically significant CME, with a decrease in the visual acuity, following modern cataract surgery has been reported at a rate from 0.2% to 14% [2, 13]. Fundus fluorescein angiography (FFA) is the gold standard for the diagnosis of CME. However, as FFA is an invasive and qualitative method, to detect CME without a decrease in visual acuity, there is a tendency to use noninvasive and quantitative methods. OCT and FAF are good, noninvasive, quantitative, and reproducible methods that are used currently.

FFA was compared with OCT by Mitne et al. for the diagnosis of CME, who found an 88% correlation between the two methods [14]. The same comparison was performed by Antcliff et al. who reported that the sensitivity and specificity of OCT was 96% and 100%, respectively [15].

In a study carried out by Perente et al. involving 102 patients who underwent phaco and PCIOL implantation, the CMT (measured using OCT) increased significantly between 1 month and 6 months, postoperatively [16]. In a similar study, Jagow et al. observed a moderate increase in the macular thickness between the 1st week and 6th week, postoperatively, but there was no significant correlation between the CMT and BCVA [17]. Using OCT,Sourdille and Santiago found an association between the increase in the CMT and the decrease in vision after the 1st week postoperative [18].

In the present study, CME has been noticed using OCT in 7.5% of patients after surgery. All of these patients had an unsatisfactory increase in visual acuity. The mean age of the patients with CME was higher than those without CME. This is consistent with publications advocating that aging may predispose the development of CME [19]. Furthermore, the CMT of those patients without CME increased significantly on day 1 following surgery, compared to the preoperative values, using OCT. Light exposure during surgery may explain the increase of the CMT in these patients.

FAF is a new and useful tool for obtaining information on baseline fluorescence from the RPE, as caused by lipofuscin. Lipofuscin mainly accumulates as a result of incomplete destruction of the outer segments of the photoreceptors. A further cause of HAF is inflammation, which triggers the pro-oxidative pathway. FAF is used for diagnosing age-related macular degeneration, hereditary retinal diseases, such as Stargardt disease, retinitis pigmentosa, and cone dystrophies [20, 21].

Displacement of macular pigments due to cystoid gaps in the CME may lead to HAF. Holz et al. stated that extracellular fluid containing retinoid proteins emits autofluorescence. Therefore, in addition to the accumulation of lipofuscin, HAF may be caused by extracellular liquid in the presence of macular edema [9, 10, 22].

FFA and FAF were carried out by McBain et al. in 34 patients suspected of having CME [23]. The sensitivity and specificity of FAF was found to be 81% and 69%, respectively, for the diagnosis of CME. Macaluso et al. and Camparini et al. evaluated patients with CME that developed due to various reasons [24, 25]. They observed a consistency between FAF and FFA in all cases. Similarly, in a further study involving 14 patients, FFA and FAF were found to be correlated with the CME [26].

Peng and Su reported that the correlation between FAF and FFA was 87% in the CME from patients with different origins [27]. Similarly, Pece et al. and Vujosevic et al. reported the HAF as 64.7% and 76.8%, respectively [28, 29].

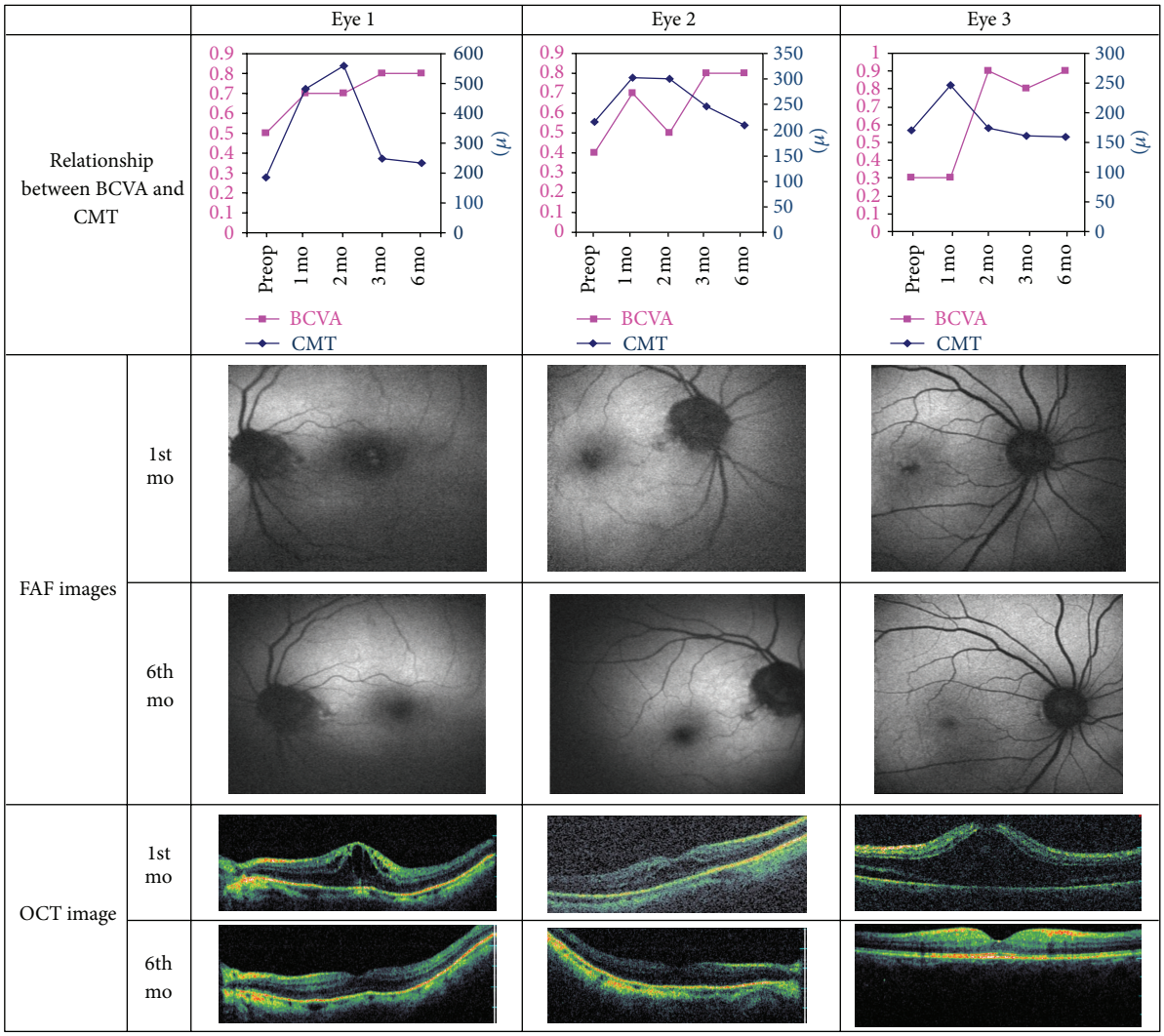

Figure 1: Fundus autofluorescence and optical coherent tomography images and the relationship between the best corrected visual acuity and central macular thickness of the eyes with CME. BCVA: best corrected visual acuity; FAF: fundus autofluorescence; OCT: optic coherence tomography; Preop: preoperative; Postop: postoperative; mo: month.

FAF has some limitations in CME. There is a correlation between the size of the cyst and HAF in CME [8]. Severity of the CME which may be seen as leakage in FA and as increased foveal thickness in OCT also exhibit significant correlation with HAF [28, 29]. So, small-sized cysts with relatively thinner fovea may not be visualized in FAF. HAF in CME is usually apparent under 488 nm excitation while may not be seen under 580 nm excitation [26]. In the current study, one of the eyes with CME could not be detected with FAF image. While we used HRA which has 488 nm excitation, we suggested that this was associated with the small size of the cyst in this eye.

In our study, HAF could not be detected in the eyes without CME. However, HAF was detected in two of the three eyes with CME and was also observed using OCT. The abnormalities in these three eyes were resolved following treatment.

Furthermore, we found that the moderate increase in the CMT in the first 3 months did not cause a decrease in the visual acuity in the patients without CME, and the thickness of the macula gradually decreased and returned to preoperative values within 3 months after surgery. The increased CMT values were regressed in the patients with CME, and HAF also disappeared as a result of the medical treatment, and after 6 months there was no permanent vision loss in any of the eyes.

However, the results of our study are somewhat limited due to the small number of patients and lack of a control group. Nevertheless our results were comparable with the results of the previous studies particularly in demonstration of the relationship between the cyst size and HAF.

In conclusion, in the evaluation of the macula in patients who underwent uncomplicated phaco surgery, HAF was correlated with OCT, demonstrating that HAF can be used

as a noninvasive, fast, and convenient method for diagnosis and followup, in the absence of OCT.

Acknowledgment

The authors thank Alparslan Sahin, MD, for his scientific assistance and critical revision of the paper.

References

[1] J. C. Norregaard, P. Bernth, L. Bellan et al., "Intraoperative clinical practice and risk of early complications after cataract extraction in the United States, Canada, Denmark, and Spain," *Ophthalmology*, vol. 106, no. 1, pp. 42–48, 1999.

[2] M. Wegener, P. H. Alsbirk, and K. Hojgaard-Olsen, "Outcome of 1000 consecutive clinic- and hospital-based cataract surgeries in a Danish county," *Journal of Cataract and Refractive Surgery*, vol. 24, no. 8, pp. 1152–1160, 1998.

[3] P. G. Ursell, D. J. Spalton, S. M. Whitcup, and R. B. Nussenblatt, "Cystoid macular edema after phacoemulsification: relationship to blood- aqueous barrier damage and visual acuity," *Journal of Cataract and Refractive Surgery*, vol. 25, no. 11, pp. 1492–1497, 1999.

[4] D. Huang, E. A. Swanson, C. P. Lin et al., "Optical coherence tomography," *Science*, vol. 254, no. 5035, pp. 1178–1181, 1991.

[5] J. A. Izatt, M. R. Hee, E. A. Swanson et al., "Micrometer-scale resolution imaging of the anterior eye in vivo with optical coherence tomography," *Archives of Ophthalmology*, vol. 112, no. 12, pp. 1584–1589, 1994.

[6] C. A. Puliafito, M. R. Hee, C. P. Lin et al., "Imaging of macular diseases with optical coherence tomography," *Ophthalmology*, vol. 102, no. 2, pp. 217–229, 1995.

[7] J. S. Schuman, M. R. Hee, C. A. Puliafito et al., "Quantification of nerve fiber layer thickness in normal and glaucomatous eyes using optical coherence tomography: a pilot study," *Archives of Ophthalmology*, vol. 113, no. 5, pp. 586–596, 1995.

[8] N. Ebrahimiadib and M. Riazi-Esfahani, "Autofluorescence imaging for diagnosis and follow-up of cystoid macular edema," *Journal of Ophthalmic & Vision Research*, vol. 7, no. 3, pp. 261–267, 2012.

[9] F. G. Holz, "Autofluorescence imaging of the macula using confocal scanning laser ophthalmoscopy," *Ophthalmologe*, vol. 98, no. 1, pp. 10–18, 2001.

[10] S. Schmitz-Valckenberg, F. G. Holz, A. C. Bird, and R. F. Spaide, "Fundus autofluorescence imaging: review and perspectives," *Retina*, vol. 28, no. 3, pp. 385–409, 2008.

[11] W. J. Stark Jr., A. E. Maumenee, and W. Fagadau, "Cystoid macular edema in pseudophakia," *Survey of Ophthalmology*, vol. 28, supplement, pp. 442–451, 1984.

[12] S. R. Irvine, "A newly defined vitreous syndrome following cataract surgery," *American Journal of Ophthalmology*, vol. 36, no. 5, pp. 599–619, 1953.

[13] S. J. Kim and N. M. Bressler, "Optical coherence tomography and cataract surgery," *Current Opinion in Ophthalmology*, vol. 20, no. 1, pp. 46–51, 2009.

[14] S. Mitne, A. Paranhos Júnior, A. P. S. Rodrigues et al., "Agreement between optical coherence tomography and fundus fluorescein angiography in post-cataract surgery cystoid macular edema," *Arquivos Brasileiros De Oftalmologia*, vol. 66, no. 6, pp. 771–774, 2003.

[15] R. J. Antcliff, M. R. Stanford, D. S. Chauhan et al., "Comparison between optical coherence tomography and fundus fluorescein angiography for the detection of cystoid macular edema in patients with uveitis," *Ophthalmology*, vol. 107, no. 3, pp. 593–599, 2000.

[16] I. Perente, C. A. Utine, C. Ozturker et al., "Evaluation of macular changes after uncomplicated phacoemulsification surgery by optical coherence tomography," *Current Eye Research*, vol. 32, no. 3, pp. 241–247, 2007.

[17] B. Jagow, C. Ohrloff, and T. Kohnen, "Macular thickness after uneventful cataract surgery determined by optical coherence tomography," *Graefe's Archive for Clinical and Experimental Ophthalmology*, vol. 245, no. 12, pp. 1765–1771, 2007.

[18] P. Sourdille and P. Y. Santiago, "Optical coherence tomography of macular thickness after cataract surgery," *Journal of Cataract and Refractive Surgery*, vol. 25, no. 2, pp. 256–261, 1999.

[19] P. Desai, D. C. Minassian, and A. Reidy, "National cataract surgery survey 1997-8: a report of the results of the clinical outcomes," *British Journal of Ophthalmology*, vol. 83, no. 12, pp. 1336–1340, 1999.

[20] R. F. Spaide, "Fundus autofluorescence and age-related macular degeneration," *Ophthalmology*, vol. 110, no. 2, pp. 392–399, 2003.

[21] B. Wabbels, A. Demmler, K. Paunescu, E. Wegscheider, M. N. Preising, and B. Lorenz, "Fundus autofluorescence in children and teenagers with hereditary retinal diseases," *Graefe's Archive for Clinical and Experimental Ophthalmology*, vol. 244, no. 1, pp. 36–45, 2006.

[22] A. Bindewald, J. J. Jorzik, F. Roth, and F. G. Holz, "cSLO digital fundus autofluorescence imaging: improvements in imaging using confocal scanning laser ophthalmoscopy," *Ophthalmologe*, vol. 102, no. 3, pp. 259–264, 2005.

[23] V. A. McBain, J. V. Forrester, and N. Lois, "Fundus autofluorescence in the diagnosis of cystoid macular oedema," *British Journal of Ophthalmology*, vol. 92, no. 7, pp. 946–949, 2008.

[24] C. Macaluso, S. Tedesco, N. Ungaro, E. Delfini, and M. Camparini, "A HRA study of retinal autofluorescence in cystoid macular edema," *Investigative Ophthalmology & Visual Science*, vol. 45, no. 5, Article ID 3014, 2004.

[25] M. Camparini, P. Cassinari, and C. Macaluso, "Autofluorescence of cystoid macular edema. A HRA scanning laser ophthalmoscope study," *Invest. Ophthalmol. Vis. Sci*, vol. 44, no. 5, Article ID 4952, 2003.

[26] K. Bessho, F. Gomi, S. Harino et al., "Macular autofluorescence in eyes with cystoid macula edema, detected with 488 nm-excitation but not with 580 nm-excitation," *Graefe's Archive for Clinical and Experimental Ophthalmology*, vol. 247, no. 6, pp. 729–734, 2009.

[27] X. J. Peng and L. P. Su, "Characteristics of fundus autofluorescence in cystoid macular edema," *Chinese Medical Journal*, vol. 124, no. 2, pp. 253–257, 2011.

[28] A. Pece, V. Isola, F. Holz, P. Milani, and R. Brancato, "Autofluorescence imaging of cystoid macular edema in diabetic retinopathy," *Ophthalmologica*, vol. 224, no. 4, pp. 230–235, 2010.

[29] S. Vujosevic, M. Casciano, E. Pilotto, B. Boccassini, M. Varano, and E. Midena, "Diabetic macular edema: fundus autofluorescence and functional correlations," *Investigative Ophthalmology and Visual Science*, vol. 52, no. 1, pp. 442–448, 2011.

Hindawi Publishing Corporation
Journal of Ophthalmology
Volume 2013, Article ID 634351, 11 pages
http://dx.doi.org/10.1155/2013/634351

Clinical Study

Multimodal Imaging in Hereditary Retinal Diseases

Francesco Pichi,[1] Mariachiara Morara,[2] Chiara Veronese,[2] Paolo Nucci,[1] and Antonio P. Ciardella[2]

[1] *San Giuseppe Hospital, University Eye Clinic, Via San Vittore 12, 20123 Milan, Italy*
[2] *Sant'Orsola-Malpighi Hospital, Ophthalmology Unit, Via Palagi 9, 40138 Bologna, Italy*

Correspondence should be addressed to Francesco Pichi; ilmiticopicchio@gmail.com

Received 5 January 2013; Accepted 31 March 2013

Academic Editor: Atsushi Hayashi

Introduction. In this retrospective study we evaluated the multimodal visualization of retinal genetic diseases to better understand their natural course. *Material and Methods*. We reviewed the charts of 70 consecutive patients with different genetic retinal pathologies who had previously undergone multimodal imaging analyses. Genomic DNA was extracted from peripheral blood and genotyped at the known locus for the different diseases. *Results*. The medical records of 3 families of a 4-generation pedigree affected by North Carolina macular dystrophy were reviewed. A total of 8 patients with Stargardt disease were evaluated for their two main defining clinical characteristics, yellow subretinal flecks and central atrophy. Nine male patients with a previous diagnosis of choroideremia and eleven female carriers were evaluated. Fourteen patients with Best vitelliform macular dystrophy and 6 family members with autosomal recessive bestrophinopathy were included. Seven patients with enhanced s-cone syndrome were ascertained. Lastly, we included 3 unrelated patients with fundus albipunctatus. *Conclusions*. In hereditary retinal diseases, clinical examination is often not sufficient for evaluating the patient's condition. Retinal imaging then becomes important in making the diagnosis, in monitoring the progression of disease, and as a surrogate outcome measure of the efficacy of an intervention.

1. Introduction

Evaluation of the retina is a critical step in understanding and diagnosing genetic disease. Because ophthalmologists can view the retina directly, they are often able to make diagnoses without additional testing. In a number of diseases, however, the clinical examination is not sufficient for evaluating the patient's condition. Retinal imaging then becomes important in making the diagnosis and in monitoring the progression of disease. It may be used to document and quantify a patient's symptoms; it may help in making a differential diagnosis of some retinal disorders, in distinguishing localized macular disorders from diffuse retinal disorders, and in distinguishing optic nerve disease from retinal disease. Early alteration of retinal imaging might serve as a surrogate outcome measure of the efficacy of an intervention, rather than waiting for years to determine if a disease has progressed clinically.

Diagnostic imaging procedures used for evaluation and followup of retinal genetic disease include colour fundus photography, blue fundus autofluorescence (FAF) [1–3], fluorescein angiography (FA) [4, 5], indocyanine green angiography (ICGA) [6], and spectral-domain optical coherence tomography (SD-OCT) [5, 7, 8].

We evaluate here the multimodal visualization of retinal genetic diseases and correlate FAF, FA, and ICG of study lesions with SD-OCT to assess their ultrastructural characteristics and to better understand the natural course of the diseases [7].

2. Methods

We reviewed the charts of 70 consecutive patients with different genetic retinal pathologies visited at the Ocular Genetic Department of the Sant'Orsola-Malpighi Hospital, Bologna, between January 2008 and December 2012. Only eyes having previously undergone multimodal imaging analyses (high-resolution digital colour fundus photographs, FAF, FA, ICGA,

and SD-OCT) were included. All patients underwent a complete ophthalmologic examination, including measurement of best-corrected visual acuity (BCVA) using standard Early Treatment of Diabetic Retinopathy Study (ETDRS) charts, slit lamp examination of the anterior segment, and fundus biomicroscopy. Colour fundus photographs were obtained using a high-resolution digital retinal camera (Topcon TRX-50 retinal camera; Tokyo, Japan). For high-resolution multimodal fundus imaging analysis, we used a combined instrument (Spectralis HRA-OCT, Heidelberg Engineering, Heidelberg, Germany) that allows for simultaneous recording of cSLO and SD-OCT images. A standardized imaging protocol was performed in all patients, which included acquisition of blue FAF and FA (excitation $k = 488$ nm; emission $k > 500$ nm; field of view, $30^\circ \cdot 30^\circ$; image resolution $768 \cdot 768$ pixels), simultaneous SD-OCT scanning using a second, independent pair of scanning mirrors ($k = 870$ nm; acquisition speed, 40.000 A-scans per seconds; scan depth, 1.8 mm; digital depth resolution, approximately 3.5 μm per pixel; optical depth resolution, 7 μm; lateral optical resolution, 14 μm), and indocyanine green angiography (excitation $k = 787$ nm; emission $k > 800$ nm; field of view, $30^\circ \cdot 30^\circ$; image resolution, $768 \cdot 768$ pixels) [7]. Fundus autofluorescence, FA, ICGA, and SD-OCT images were evaluated on a computer monitor by two independent examiners (F.P. and M.M.).

Genomic DNA was extracted from peripheral blood with the Qiagen Blood DNA extraction kit (Qiagen, Crawley, UK) and genotyped at the known locus for the different diseases using short tandem repeat polymorphisms [9]. DNA samples were subsequently examined with a genome-wide scan of single nucleotide polymorphisms and the genotypes that were produced were studied with linkage and haplotype analyses [10].

3. Results

3.1. North Carolina Macular Dystrophy (NCMD). The medical records of 3 families of a 4-generation pedigree were reviewed; the first recorded examination period took place in 2009, and the last took place in 2012. Twelve members were found to be clinically affected with NCMD. Macular findings among the affected patients ranged from disease grade 1 (6 eyes, mean age 57 years old) to grades 2 (8 eyes, mean age 44 years old) and 3 (10 eyes, mean age 19 years old) (Figure 1). All affected patients had symmetric disease grades bilaterally; when first examined, those with disease grade 2 had a median VA of 20/25 and those with disease grade 3 had a median VA of 20/60. In addition, all affected family members had numerous yellow, midperipheral drusen-like deposits in both eyes.

Genetic testing of family members mapped the responsible mutation to the MCDR1 locus on chromosome 6 between the markers D6S1609 and D6S1627.

Grade 1 lesions showed clusters of peculiar, yellow-white spots at the level of the RPE; angiography revealed a pattern of hyperfluorescence that was apparent in the arterial phase and did not change during the course of angiography. The drusen-like lesions could not be picked up by SD-OCT, but where hyperautofluorescent, suggesting a lipofuscin composition (Figure 1(a)).

Grade 2 lesions consisted of substantial disciform scarring, often resulting from CNV; autofluorescence imaging showed a ring of increased autofluorescence, surrounded by a ring of decreased autofluorescence corresponding to the ring of mottled RPE. Spectral domain OCT showed loss of architecture of the outer retina due to fibrotic CNV, without activity on FA (Figure 1(b)).

Grade 3 lesions consisted of excavated atrophic chorioretinal lesions with an overhanging lip of retina that partly surrounded these lesions; these features were confirmed by autofluorescence, that showed loss of central autofluorescence with a ring of hyperautofluorescence at the edge of the lesions. Angiography revealed the presence of only a few small choroidal blood vessels in the area of the macular lesions, surrounded by subretinal fibrosis (Figure 1(c)).

3.2. Stargardt Disease. A total of 16 eyes (8 patients) with Stardardt disease were retrospectively reviewed; there were 5 women and 3 men with a mean age at presentation of 39 years (range 17–46 years). Best-corrected visual acuity ranged from 20/20 to 20/400, with a mean of 20/80.

Two main defining clinical characteristics of the disease were identified in our patients: 7 eyes (43.7%) presented with yellow subretinal flecks, 5 eyes (31.2%) showed central atrophy, and 4 eyes (25.1%) a combination of the previous lesions.

On colour fundus photography, the retinal flecks presented heterogeneous patterns, which were perifoveal or widely distributed in the fundus (Figure 2). Flecks corresponded on FAF imaging to areas where the autofluorescence signal differed from the overall background level (Figure 2(b)). Most flecks seen on FAF were hyperautofluorescence, whereas some were surrounded by a ring of decreased autofluorescence. On FA the characteristic pisiform flecks were hypo- or hyperfluorescent (Figure 2(d)). Spectral Domain OCT scans through the flecks clearly revealed 2 patterns, as described by Querques et al. [11]. Type 1 deposits are dome shaped and located at the level of or just above the RPE; type 1 deposits were observed in 91% of our patients (Figure 2(b), square a). Type 2 deposits presented as small, linear hypoerreflective lesions located at the level of the inner segments of photoreceptors or outer nuclear layer (ONL) and clearly separated from the RPE; type 2 lesions were observed in 84% eyes (Figure 2(b), square b). The number of flecks located in the macula increased radially exhibiting a pattern of centrifugal addition beginning from the fovea and extending toward the outer edges of the macula; newer flecks appeared hyperautofluorescent on FAF imaging, while older flecks become progressively more hypoautofluorscent with time.

Central atrophy corresponded to a clearly demarcated area of uniform decreased autofluorescence surrounded by a border of patchy, mottled hypoautofluorescence (Figure 2(b)); the sharply demarcated areas of central atrophy gradually enlarged in 3 eyes, and new areas of atrophy appeared to emerge and extend selectively into locations demonstrating mottled hypoautofluorescence. Angiography demonstrated perifoveal window defect, corresponding to dropout of RPE cells, and visualization of the large choroidal vessels centrally (Figure 2(d)).

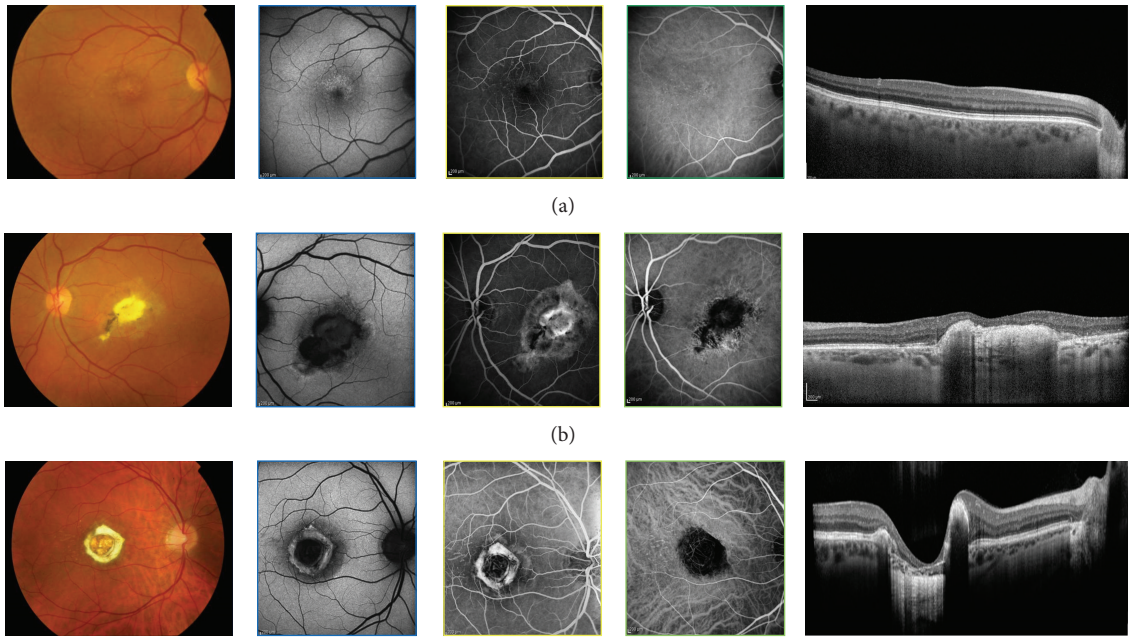

(a)

(b)

(c)

Figure 1: Fundus photographs of affected patients with North Carolina macular dystrophy, showing fine, confluent drusen in the macula (grade I), a subretinal scar due to a prior choroidal neovascularization (Grade II), and a macular caldera (Grade III). In Grade I lesion, autofluorescence shows marked hyperautofluorescence of the bright drusen-like elements. SD-OCT shows a normal anatomy of the inner retina; the photoreceptor-retinal pigment epithelium complex appears normal, and the drusen-like lesions are not detectable. In Grade II lesion, SD-OCT shows increased reflectivity consistent with subretinal fibrosis or gliosis. In the Grade III lesion, fundus autofluorescence demonstrates central hypoautofluorescence, surrounded by normal appearing retina tissue and preserved foveal tissue. There is a hyperautofluorescent perimeter surrounding the edges of the lesion, possibly indicative of metabolic byproduct deposition. SD-OCT demonstrates a normal hyperreflective IS/OS photoreceptor junction with abrupt attenuation of outer retinal structures and RPE absence within the lesion.

An angiographically dark choroid was noted in 62% of our patients (Figure 2(d)); the lack of early choroidal flush is thought to be due to blocking of choroidal fluorescence by a diffuse accumulation of lipofuscin in the RPE.

3.3. Choroideremia. Medical records of nine male patients with a previous diagnosis of choroideremia were reviewed; mean age was 23 years old, and mean BCVA at presentation was 20/30. The disease was bilateral and symmetric in 9/9 (100%) patients. Three patients (33.3%) showed midperipheral RPE abnormalities, which in 5 patients (55.5%) had already spread peripherally with involvement of the choroid too and visualization of coursing large choroidal vessels; one patient (11.1%) presented with vascular attenuation and optic atrophy (Figure 3). The fovea was spared in every case. In 100% of the patients, FA showed filling of the retinal and large choroidal vessels, but not of the choriocapillaris. The intact fovea was hypofluorescent and surrounded by a hyperfluorescence stellate preservation of the posterior pole due to an extensive window defect. Zonal areas of peripheral atrophy were accentuated on the FAF as areas of hypoautofluorescence, which contrasted with the physiological autofluorescence of the fundus (Figure 3(b)). Spectral domain OCT scans showed diffuse choroidal atrophy and loss of the IS/OS junction, which was intact and preserved at the level of the fovea (Figure 3(c)).

Eleven female carriers of the 9 independent families were examined, 9 mothers and 2 sisters. Mean BCVA was 20/25. All carriers (100%) showed mild, patchy peripheral RPE atrophy and mottling with a striking speckled pattern in FAF and simultaneous choroidal and retinal filling in FA (Figures 3(d), 3(e), 3(f), and 3(g)).

3.4. Bestrophinopathies . Fourteen patients with Best vitelliform macular dystrophy (BVMD) were included. The mean age of enrolled subjects was 37 years (range 9 to 59 years). The median BCVA was 20/50 (range 20/20 to 20/320).

In 2 patients with a positive family history of BVMD, clinical evaluation showed RPE mottling and SD-OCT imaging demonstrated a prominent highly reflective material between the RPE/Bruch's membrane complex and the IS/OS junction (previtelliform stage, Figure 4(b)).

In 5 patients, an elevated yellow round macular lesion measuring approximately 3/4 disc diameter across was found in the fundus. On SD-OCT imaging, the foveal retina was elevated due to a homogeneous hyperreflective material located just above the RPE. The hyperreflective material presented increased fluorescence on FAF (vitelliform stage, Figure 4(a)).

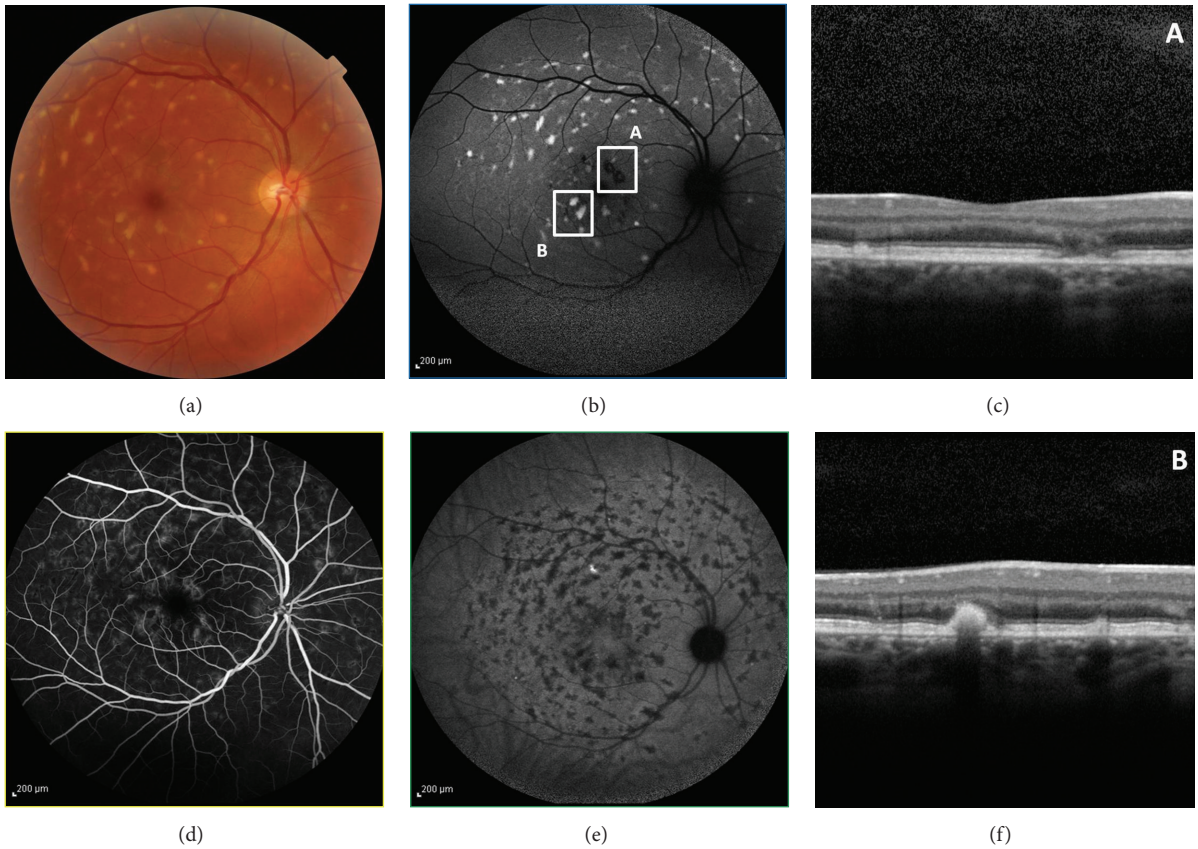

Figure 2: Color photograph shows macular atrophy and retinal flecks in a Stargardt patient. OCT scans are illustrated by the arrows 1 and 2. The autofluorescent frame clearly delineates the retinal flecks. Thin and open arrows point to two of the flecks, respectively, crossed by scans 1 and 2. Fluorescein angiography shows the dark choroid appearance, and the hypofluorescent flecks are hardly discernable in the hyperfluorescent background because of RPE changes. On ICG, late phase (30 min), the hypofluorescent lesions appear more numerous than the autofluorescent flecks, and there is sparing of the peripapillary area. The SD-OCT scan in square A shows a small hyperreflective lesion located at the inner part of the RPE layer, called type 1 deposit, and macular atrophy. The SD-OCT scan in square B shows a small hyperreflective linear lesion located at the level of the outer nuclear layer and clearly distinguished from the RPE layer, called type 2 deposit.

In 4 patients, an elevated oval macular lesion measuring approximately three disc diameters across was observed in both eyes. A yellowish material located more prominently at the inferior aspect of the lesion was evident. In the center of the macula, SD-OCT imaging showed separation of the neurosensory retina from the RPE by an optically clear space and clumps of homogeneous hyperreflective material overlying the RPE inferiorly displaced. On FAF, increased autofluorescence from the hyperreflective material overlying the RPE was observed from the inferior aspect of the lesion (pseudohypopyon stage, Figure 4(c)).

In 3 patients elevated macular lesions, with variable amounts of yellowish subretinal material dispersed within, were observed. SD-OCT imaging showed the neurosensory retina separated from the RPE centrally by an optically clear space, photoreceptors' OS irregularly elongated, and hyperreflective mounds at the level of the RPE, clearly delineated on FAF (vitelliruptive stage, Figure 4(d)).

Two of the previous patients had family members with DNA samples available for study, and in each of these families, the disease causing variations were found to lie on separate alleles, consistent with autosomal recessive bestrophinopathy (ARB). Six patients with ARB from 2 nonconsanguineous families were therefore reviewed. All patients had bilateral maculopathy with subretinal yellow deposits. Subretinal deposits in subjects 3 to 6 were more prominent, appearing as multifocal, round, yellow lesions surrounding a macular neurosensory retinal detachment (Figures 5(a) and 5(d)). Similar additional areas of 2 to 3 disc diameters were present above the optic discs. In all patients, fundus autofluorescence imaging displayed marked hyperautofluorescence corresponding to the yellow lesions (Figures 5(c) and 5(f)). In subject 2, this identified additional peripapillary hyperfluorescent deposits not seen on funduscopy. Spectral-domain optical coherence tomography scans demonstrated round- or dome-shaped deposits within the RPE reaching into the subretinal space in all subjects, which extended up to the OPL (Figure 5(b)). The RPE itself was thinned throughout the macula. Photoreceptor outer segments were thicker and elongated compared with normal control data. Small filament-like bridges were visible between the photoreceptor outer segment layer and the RPE (Figure 5(e)). Verhoeff's membrane, the interface between

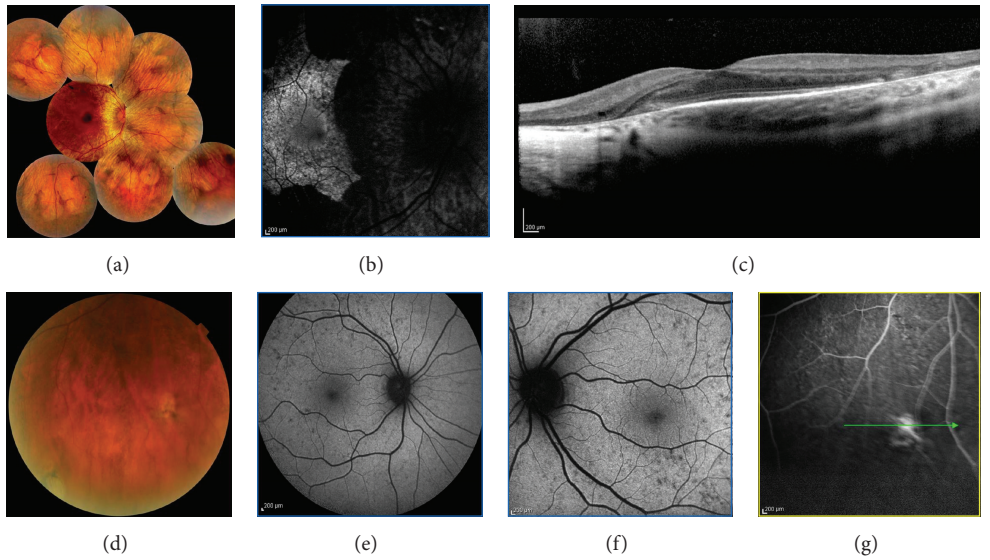

Figure 3: Fundus photograph of a male patient affected by choroideremia shows midperipheral RPE atrophy spreading peripherally with visualization of coursing large choroidal vessels and sparing of the fovea. Fundus autofluorescence demonstrates an hyperautofluorescent stellate preservation of the posterior pole. Spectral-domain OCT scans show diffuse choroidal atrophy and loss of the IS/OS junction, which is intact and preserved at the level of the fovea. The boy's mother was a genetically confirmed female carrier: her fundus shows mild, patchy peripheral RPE mottling with a striking speckled pattern in FAF.

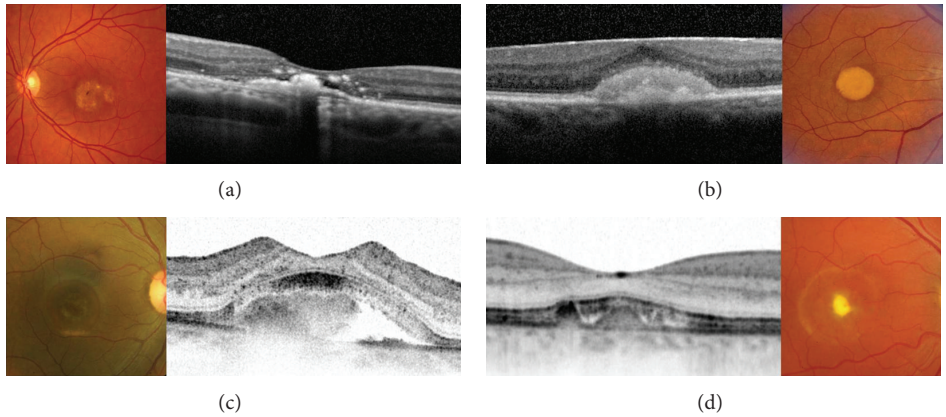

Figure 4: Spectral domain-OCT scans document the natural evolution of BVMD. Firstly a thicker layer between the photoreceptors inner/outer segment interface and the underlying RPE (previtelliform stage). The material is subsequently deposited under the neurosensory retina (vitelliform stage) and is sometimes accompanied with a neurosensory detachment (pseudohypopyon stage) secondary to its reabsorption, with abnormalities of the RPE and subsequent thinning of all retinal layers (vitelliruptive and atrophic stage).

cone photoreceptors and the RPE, was not identifiable in multiple scans. Inner retinal layers were unaffected. All subjects harbored compound heterozygous mutations in BEST1; the 2 most frequent recessive alleles observed in our series were Arg141His (3 patients) and Ala195Val (2 patients), whereas one patient had an Arg92Cys mutation.

3.5. Enhanced S-Cone Syndrome (ESCS). Seven patients with ESCS were ascertained. The clinical presentation in all patients was night blindness, with or without reduced central vision. Nyctalopia had begun in early childhood with onset ranging from 2 to 6 years of age. No patient reported photophobia. Visual acuity ranged between 20/20 and 20/80. Nystagmus was not present in any patient. Vitreous cells were present in all patients. The fundus appearance varied between patients. The youngest subject had normal appearing fundi. Six patients had subtle to mild pigmentary changes with nummular pigmentary deposition at the level of the RPE, usually located in the midperiphery along the vascular arcades and often associated with RPE atrophy, with one of these subjects having small yellow-white dots at the posterior pole (Figures 6(a) and 6(e)). Foveal schisis-like changes were observed in 6 patients. OCT demonstrated foveal cyst formation (Figures 6(d) and 6(h)). Subsequently, these patients

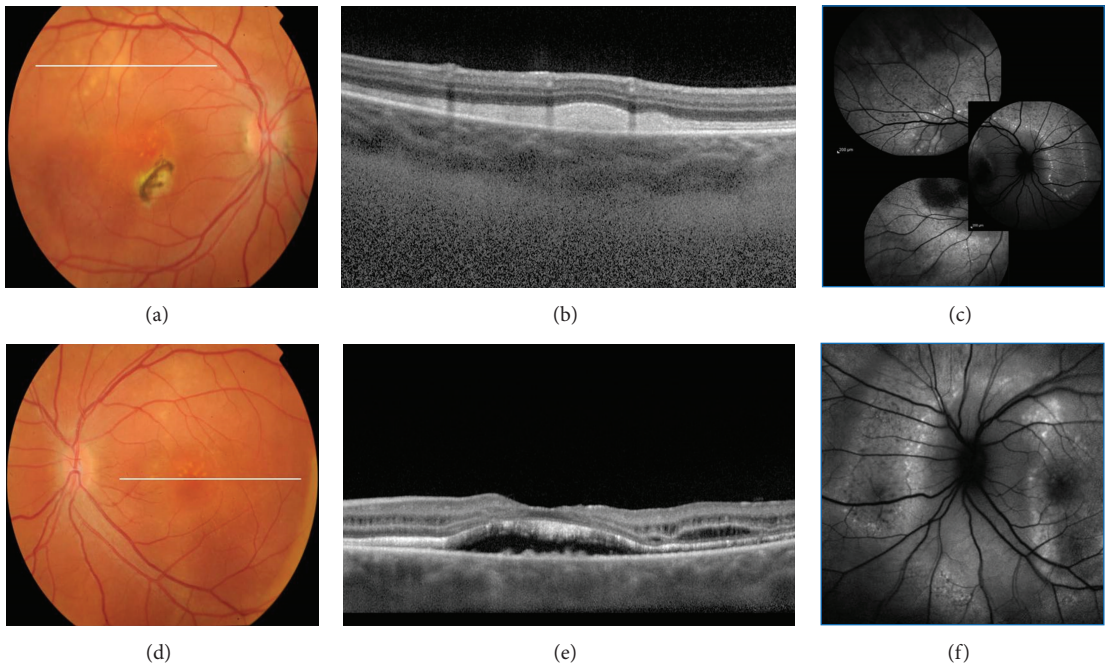

(a) (b) (c)

(d) (e) (f)

Figure 5: Fundus photograph of an autosomal recessive bestrophinopathy shows a well-demarcated area with round yellowish-white deposits at the posterior pole and along the superotemporal arcade; subretinal fibrosis is visible inferior nasal of the fovea. SD-OCT scan illustrates extensive RPE deposits extending to the outer plexiform layer. Fundus autofluorescence imaging displayed marked hyperautofluorescence corresponding to the yellow lesions. Fundus photograph shows a well-demarcated area with round yellowish-white deposits at the posterior pole extending to the superior periphery. SD-OCT scan demonstrates RPE detachment from the photoreceptors. Photoreceptor outer segments are thickened and elongated. Fundus autofluorescence identified additional peripapillary hyperfluorescent deposits not seen on funduscopy.

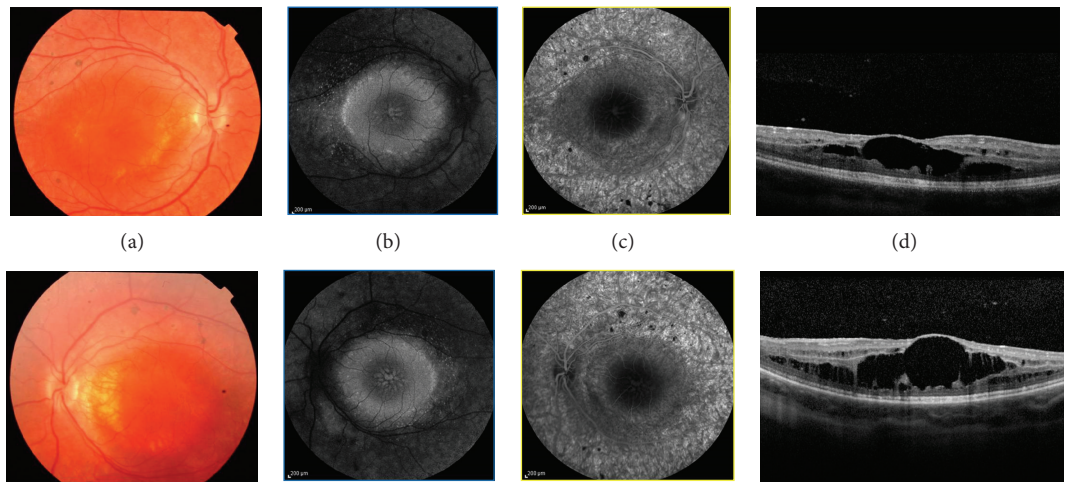

(a) (b) (c) (d)

(e) (f) (g) (h)

Figure 6: Color fundus photography of a patient with enhanced s-cone syndrome showing nummular pigmentary clumping at the level of the RPE along the vascular arcades and macular disturbance with subtle pigmentary changes; fundus autofluorescence shows an absence of AF outside the arcades and a ring of increased AF at the posterior pole. Foveal schisis is demonstrated on SD-OCT and confirmed by the absence of leakage on fluorescein angiography.

had FA, which showed no leakage, suggesting that the cystoid changes were more likely to be secondary to schisis than to edema (Figures 6(b) and 6(f)). Fundus autofluorescence showed a decrease or lack of autofluorescence outside the arcades, a ring of relatively increased autofluorescence in the transitional zone between this area of decreased/absent autofluorescence and the macular region, and a spoke-like area of relatively increased autofluorescence centered on the

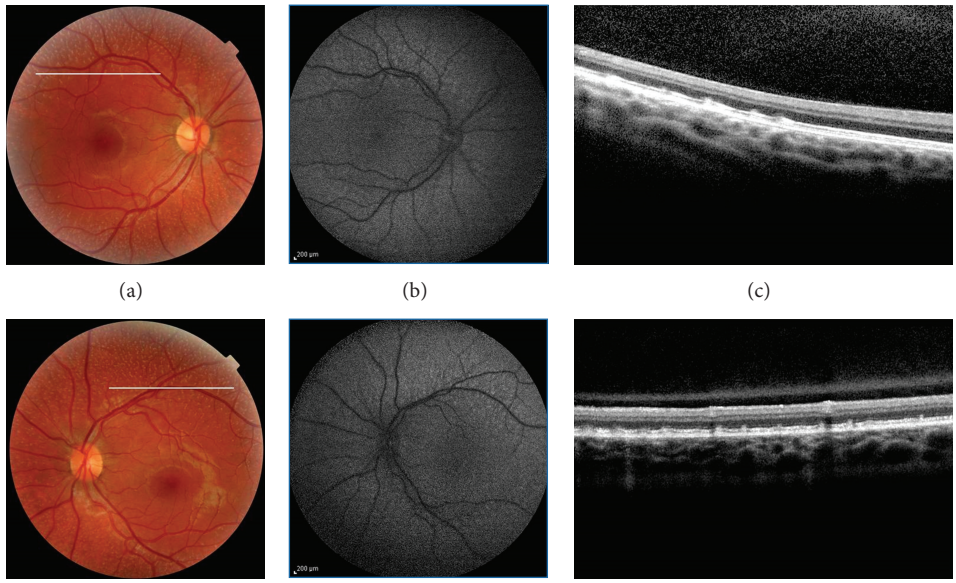

Figure 7: Fundus photograph of two eyes with fundus albipunctatus shows many small white dots scattered throughout the retina except for the foveal area. Fundus autofluorescence imaging of both eyes produced fuzzy and grainy images, and the margins of the optic nerve head and blood vessels are blurred. On SD-OCT, focal thickening centered in the photoreceptor OS and extending forward close to the outer limiting membrane and backward to the outer aspect of the RPE is seen corresponding to the multiple discrete albipunctate dots. These lesions seem to bulge their outer and inner boundaries. There was a reduced visualization of the photoreceptor outer tips.

fovea (Figures 6(c) and 6(g)). Mutations were identified in 7 of 7 subjects. Three previously reported mutations were identified, a splice acceptor intron 1 mutation (IVS1-2A>C splice site) with the Arg311Gln (R311Q) and Arg104Trp (932G → A; exon 6substitutions) and the 481delA frameshift mutation.

3.6. Fundus Albipunctatus. We included 3 unrelated patients (aged 20, 35, and 8 years) with fundus albipunctatus.

All patients had diffusely scattered white round flecks scattered in a radial pattern from the vascular arcades throughout the retina, except for the foveal area (Figures 7(a) and 7(d)). Mean BCVA was 20/25, and the results of the ocular examination were normal except for the fundus. Spectral domain OCT revealed an irregular IS band through the macula and a dome-shaped elevation corresponding to discrete albipunctate dots (Figure 7(c) and 7(f)). These elevated lesions were at the level of the RPE and extended into the IS band and external limiting membrane. The ONL thickness was thinner than that in normal controls. In 2/3 patients the FAF image was fuzzy and grainy, and the margins of the optic nerve head and blood vessels were blurred. No enhanced hyperautofluorescent spots or rings, which may correlate to the albipunctate spots on the fundus photo, were observed. Whereas fundus autofluorescence was scarcely detectable in the 2 oldest patients, it was severely reduced in the youngest (Figures 7(b) and 7(e)) but still detectable.

Two patients harbored homozygous mutations (c.881G.C and c.382G.A, resp.) and the third patient harbored the compound heterozygous mutations (c.95delT and c.712G.T) in RDH5.

4. Discussion

This study reports a comparison between FAF, FA, ICGA, and OCT for imaging of genetic retinal diseases.

North Carolina macular dystrophy is an autosomal dominant macular dystrophy with variable expressivity but complete penetrance that rarely progresses [12, 13]. Visual acuity is often better than expected from the clinical examination of the macula, ranging from 20/20 to 20/200, with a median of 20/50. Color vision, full-field electroretinography, and electrooculography results typically are normal. North Carolina macular dystrophy is unusual in its phenotypic variability and has been classified into different grades: grade 1, drusen-like yellow-white lesions in the macula at the level of the retinal pigment epithelium (RPE); grade 2, confluent drusen with or without pigmentary changes, RPE atrophy, or a disciform scar; and grade 3, staphyloma or coloboma with chorioretinal atrophy [13–15] (Figure 1). In grade 3 disease, hyperpigmentation and heaped-up white scar tissue are seen at the edge of the macular lesion. Development of choroidal neovascularization is uncommon but can worsen otherwise relatively stable visual acuity. Although grade 3 macular lesion is characteristic of NCMD, there has been much confusion in the literature regarding its nomenclature and 3-dimensional configuration. Small et al. [14] originally described these lesions as colobomas. Frank et al. [16] further studied this family and called these lesions choroidal atrophy, thereby creating some controversy. Gass [17] later described other members with NCMD as being "staphylomatous appearing." Small et al. [13] reexamined the original family and concurred

with Gass, because the cases were "clearly excavated, colobomatous, or staphylomatous in appearance when examined with binocular methods". Subsequently, grade 3 lesions were labeled and characterized as colobomas or staphylomas in the literature [15]. However, terms such as *coloboma* and *staphyloma* clearly are misnomers; *coloboma* refers to an absence of tissue that had never been present, and *staphyloma* refers to an outpouching of the sclera that is lined with uveal tissue. On review of the published literature, there has never been proof of staphyloma formation by ultrasound. In the patients with staphylomatous changes, SD-OCT showed no outpouching of the scleral tissue. Instead, on biomicroscopic and binocular ophthalmoscopic examination, there is an illusion of outpouching because of the heaped-up subretinal gliosis and fibrosis surrounding the zone of atrophy in a curvilinear pattern. Khurana et al. [15] agree with Small's initial observation of a "posterior bowing of the central macula that produced a crater-like or staphylomatous appearance. The sharply demarcated temporal edge has a ledge or overhang affect". Khurana proposed a new term for these grade 3 lesions, macular caldera. Caldera refers to a craterlike volcanic feature formed by the central collapse of land after a volcanic eruption. In our series, the SD-OCT scans of the 10 eyes with grade 3 lesions show the excavation centrally with the subretinal fibrous or gliotic tissue surrounding the atrophy, confirming that the term coined by Khurana might describe the best this lesion (Figure 1(c)). Although the pathogenesis of these grade 3 lesions is not known, Khurana proposed the following possible mechanism to describe the caldera formation. In NCMD, pathologic processes similar to those of AMD seem to begin in utero. In some cases, CNV, RPE tears, macular hemorrhaging, and eventually disciform-type lesions with fibrosis, gliosis, or both may occur. The characteristic greyish-white, heaped-up subretinal tissue that occurs at the border of the profound macular atrophy may be secondary to eruptive hemorrhaging and, subsequently, to accentuated fibrosis and gliosis and scar tissue formation. As the hemorrhage becomes organized, the authors speculate that the tremendous, inherent growth potential that characterizes virtually all fetal and neonatal tissues could result in the circumferential, heaped-up hyperplastic or hypertrophic subretinal scar.

ABCA4 is the only gene known to cause autosomal recessive Stargardt disease. Localized to the rims of rod and cone outer segments, *ABCA4* gene product (an ATP-binding cassette transporter) normally transports all-trans-retinol produced in light exposed photoreceptor outer segments to the extracellular space [11, 18]. When a mutation in the *ABCA4* gene results in a dysfunctional protein, A2E (N-retinylidene-N-retinyl-ethanolamine), derived from the retinoid component of photopigment accumulating from photoreceptor OS debris, accumulates within the photoreceptors outer segment cell membrane. Adjacent RPE cells then phagocytose shed photoreceptor outer segments engorged with cytotoxic A2E, and large amount of intracellular A2E quickly accumulates, with flecks formation. The accumulation of flecks in Stargardt patients in our series progressed spatially from the fovea in a radial pattern, suggesting that the earliest events leading to fleck formation occur close to the fovea [19]. Fleck lesions on FAF imaging were observed to increase in hyperautofluorescence, reach a peak, then decrease subsequently in autofluorescence to near-background levels, and eventually become hypoautofluorescent. The hyperreflective deposits at the level of the ONL (type 2) could be the residual cover of the dome-shaped lesions (type 1). This latter hypothesis is consistent with the natural history of the flecks, which progressively degrade, from a well-defined lesion to residual material.

A2E laden RPE exhibits impaired degradation of phospholipids, which induces the release of proapoptotic proteins from mitochondria [18] and deterioration with the breakdown of cellular membranes and the ultimate lysis and death of RPE cell which may culminate in atrophy. ICGA may provide useful information about alterations of the choroid and the choriocapillaris [11]. The finding of hypocyanescence by ICGA in advanced disease ("dark atrophy" as previously described by Giani et al.) may be due to extended damage to choriocapillaris [20]. Moreover, the absence of normal choroidal hyperfluorescence by FA in the final stages, described by Yzer et al. [21] as "choroidal silence," is due to marked atrophy of the choriocapillaris, which is a direct consequence of RPE absence. The choroid under the areas of atrophy seems to be morphologically intact.

Dark choroid is characterized by the absence of normal background fluorescence mainly due to the presence of RPE lipofuscin that absorbs the blue excitatory light [20].

Choroideremia is caused by mutations in the CHM gene localized to the long arm of X-chromosome (Xq21.2). The mutation affects the production of Rab escort protein isoform 1 (REP-1), the enzyme that plays a key role in the activation of Rab proteins that are responsible for the regulation of exocytic and endocytic cellular pathways. Boys have difficulty seeing at night in the first decade of life and then become aware of loss of peripheral vision by their teens. Areas of RPE disruption throughout the fundus are early clinical manifestations in a male patient with choroideremia (Figures 3(a), 3(b), and 3(c)). The progressive retinal changes in choroideremia can be described by careful analysis of SD-OCT images [22]. In the early phase, retinal thickening occurs with normal laminae, possibly due to Müller cell activation and hypertrophy creating interlaminar bridges. Late phases show shortening of the inner and outer segments, reduced thickness of the outer nuclear layer, and depigmentation of the RPE. Areas of chorioretinal atrophy become evident over time with loss of choriocapillaris, exposure of choroidal vessels, and loss of the RPE beyond the macula. In most cases central visual acuity is well maintained until quite late in the course of the disease, despite substantial loss of peripheral vision and significant chorioretinal degeneration [22].

Female choroideremia carriers can be identified clinically by the presence of patchy areas of RPE atrophy (Figures 3(d), 3(e), 3(f), and 3(g)) [23]. Fluorescein angiography has been advocated as a supplemental examination to detect female carriers by demonstrating window defect in the RPE. Furthermore, instead of an initial appearance of a choroidal flush, the choroidal circulation is delayed such that the retinal circulation and the choroidal circulation appear to fill simultaneously [24]. Fundus autofluorescence provides

predictive information for the detection of female carriers. A characteristic pattern of granular high-density FAF with low-density fluorescence spots was present throughout the examined area in the female carriers included in this study. This pattern is due to the fact that the CMH gene product (REP1) is localized in rods and RPE cells, but not in cones [24]. Therefore, a patch of degeneration in a CMH carrier fundus may either arise from a clone of rod cells or RPE cells with the inactivated wild-type REP1 gene; X-linked disorders show independent degeneration of RPE cells and rods show irregularly distributed changes of hypo- (degenerating RPE) and hyperautofluorescence (degenerating rods).

Best vitelliform macular dystrophy was the first inherited retinal condition in which mutations in the *BEST1* gene were shown to be the underlying cause. Other mutations in the same gene are known to cause ARB. Hence this group of conditions is called *bestrophinopathies*. Common to all, the primary pathogenetic mechanism seems to be situated at the level of the RPE, with secondary photoreceptors involvement.

BVMD is caused by missense mutation in the *BEST1* gene, located on chromosome 11q13 and containing 11 exons. BEST1 encodes bestrophin-1, a protein localized to the basolateral surface of the RPE, where it forms chloride channels [25]. Even if fundoscopic appearance and progression of BVMD have been fully described, and FA and ICGA do not add any further significant information, the advent of novel imaging techniques such as fundus autofluorescence has confirmed that the yellowish intra- and subretinal material is hyperautofluorescent, due to its high lipofuscin content [26] (Figure 4). Data obtained with SD-OCT have suggested that material seen on fundoscopy as vitelliform material is located under the neurosensory retina rather than in and under the RPE [27]. Tomographic scans firstly show a thicker layer between the photoreceptors inner/outer segment interface and the underlying RPE (previtelliform stage). Material is subsequently deposited under the neurosensory retina (vitelliform stage) and is sometimes accompanied with a neurosensory detachment (pseudohypopyon stage), with abnormalities of the RPE and subsequent thinning of all retinal layers (vitelliruptive and atrophic stages). On the basis of OCT and FAF findings, Spaide et al. [27] has hypothesized a pathogenetic mechanism: inadequate removal of subretinal fluid leads to the physical separation of the photoreceptors from the underlying RPE; this results in the progressive accumulation of lipofuscin at the outer side of the neurosensory retina due to shedding of the outer segment discs without proper phagocytosis by the RPE cells; with time, atrophy of the photoreceptors and thinning of the accumulated material lead to a decrease of the hyperautofluorescence, eventually damage to the RPE ensues.

ARB is due to compound heterozygous or homozygous mutations in BEST1 and segregates as an autosomal recessive trait [28]. ARB has been hypothesized to represent the BEST1 null phenotype, with either very little or no functional bestrophin-1 available to RPE cells. Patients with ARB present with slowly progressive central visual loss, hypermetropia, irregularity of the RPE, and deep, scattered, white subretinal deposits that characteristically hyperfluoresce on FAF imaging [29] (Figure 5). Spectral-domain OCT shows RPE deposits, photoreceptor detachment, elongated and thickened photoreceptor OS, and preserved inner retinal layers.

Multimodal imaging of bestrophinopaties suggests a regional difference in expression of the bestrophin protein throughout the retina, with more protein being produced in the retinal periphery compared to the macula. This differential expression may lead to a more pronounced relative lack of functional bestrophin in the macula, which would explain why the latter is predominantly affected in BVMD.

Enhanced s-cone syndrome is a rare, slowly progressive autosomal recessive retinal degeneration related to mutation in NR2E3. NR2E3 encodes a ligand-dependent transcription factor that controls retinal progenitor cell fate. It promotes differentiation and survival of rod photoreceptors by differentially regulating transcription of rod- and cone-specific genes either directly or indirectly through interaction with other transcription factors. Mutation in NR2E3 is thought to cause disordered photoreceptor cell differentiation, possibly by encouraging default from the rod photoreceptor pathway to the s-cone pathway, thereby altering the relative ratio of cone subtypes [30]. Histopathologic data have reported an absence of rods, but a two-fold increase in the cone population, most of which were thought to be s-cones [31]. The retina was highly degenerated and disorganized. Photoreceptors were found only in the central and far peripheral regions. Densely packed cones were intermixed with inner retinal neurons [32]. The increased number of cones in ESCS is unique, since, as a group of disorders, the progressive retinal dystrophies are usually characterized by a loss of photoreceptors. The most typical ophthalmoscopic feature in our series was the presence of nummular, midperipheral pigmentary deposits at the level of the RPE (Figure 6). This typical retinal appearance was associated with an absence of FAF outside the vascular arcades, possibly relating to loss of photoreceptors in this region. A ring of relatively increased FAF in the transitional area between the region of absent FAF and the central zone of relatively normal FAF was evident. The increased FAF detected may be related to lipofuscin accumulation secondary to RPE-photoreceptor dysfunction in that area. Foveal schisis documented by FA and OCT was present in 6/7 patients, in keeping with previous findings. The typical nummular, midperipheral pigmentary changes are a useful clinical sign, but are not a consistent finding, being evident in 6/7 patients in the present series. The association of these nummular pigmentary deposits with white-yellow dots at the level of the RPE along the vascular arcades, focal hyperpigmentation within the arcades, and foveal or peripheral schisis is more suggestive of ESCS.

Fundus albipunctatus is considered to be a form of congenital stationary night blindness because of the predominant stationary nature of the disease and associated night blindness. It is caused by mutations in RDH5, encoding 11-cis-retinol dehydrogenase [33], and leads to impaired production of 11-cis retinal, restricting the photopigment turnover and leading to reduced formation of lipofuscin [34]. Therefore, the retinas of 2 patients in our series have a grainier appearance in FAF than normal retinas do [34, 35]. Recent studies support that the RPE has an alternative pathway involving RDH10 for the production of 11-cis-retinal, which

can account for the delayed dark adaptation in patients with fundus and may explain the residual remaining FAF found in the youngest of our patient [35].

The presumed accumulation of cis-retinol and cis-retinyl esters in the RPE because of 11-cis-retinol dehydrogenase deficiency is responsible for the formation of white flecks in RDH5 mutation-associated fundus albipunctatus [36, 37] (Figure 7). It is not clear, however, why such accumulation should result in highly focal rather than diffuse accumulation of material. Furthermore, SD-OCT at high spatial resolution showed that the characteristic white flecks of the fundus are located in the outer retina at a specific depth, namely, in the photoreceptor inner and OS and RPE layers where the lesions are interspersed between normal-appearing stretches of outer retina, apparently bulging the outer limiting membrane [37].

In this study, we employed a digital retinal camera and a SD-OCT system combined with a multimodal cSLO topographic imaging system to obtain color fundus photographs and simultaneous recordings of cross-sectional SD OCT and c-SLO images, to correlate FA, FAF, and ICGA images.

It should however be kept in mind that specialized retinal function and electrophysiologic testing are still fundamental to diagnose retinal genetic disease and to better understand the roles of various genes in maintaining structure and the function of the retina. For example, a normal fundus appearance and imaging do not preclude someone from carrying the disease *BEST1* gene, and an electrooculogram (EOG) should always be performed to look for a $\text{Light}_{\text{peak}}/\text{Dark}_{\text{through}}$ ratio generally less than 1.5 or 150%. As for ESCS, it must be noted that ERG recordings firstly showed that the large a-waves were nearly entirely driven by the s-cones, thus suggesting for the first time that the hypersensitivity and hyperfunction of the s-cone system were due to an increased number of s-cones.

In conclusion, genetic diseases may target the rod system or the cone system, together or independently, and multimodal imaging and electrophysiologic testing may be employed to determine the relative involvement of these two systems. As various therapies, including gene replacement, are proposed for these disorders, retinal function and imaging testing should help determine whether these treatments are beneficial in altering the natural course of a disease and whether they adversely affect retinal function.

References

[1] F. C. Delori, C. K. Dorey, G. Staurenghi, O. Arend, D. G. Goger, and J. J. Weiter, "In vivo fluorescence of the ocular fundus exhibits retinal pigment epithelium lipofuscin characteristics," *Investigative Ophthalmology and Visual Science*, vol. 36, no. 3, pp. 718–729, 1995.

[2] S. Schmitz-Valckenberg, F. G. Holz, A. C. Bird, and R. F. Spaide, "Fundus autofluorescence imaging: review and perspectives," *Retina*, vol. 28, no. 3, pp. 385–409, 2008.

[3] F. Pichi, M. Morara, C. Veronese, A. Lembo, P. Nucci, and A. P. Ciardella, "Perivenular whitening in central vein occlusion described by fundus autofluorescence and spectral domain optical coherence tomography," *Retina*, vol. 32, no. 7, pp. 1438–1439, 2012.

[4] A. E. Elsner, S. A. Burns, J. J. Weiter, and F. C. Delori, "Infrared imaging of sub-retinal structures in the human ocular fundus," *Vision Research*, vol. 36, no. 1, pp. 191–205, 1996.

[5] A. Clark, N. Balducci, F. Pichi et al., "Swelling of the arcuate nerve fiber layer after internal limiting membrane peeling," *Retina*, vol. 32, no. 8, pp. 1608–1613, 2012.

[6] F. C. Piccolino, L. Borgia, E. Zinicola, M. Iester, and S. Torrielli, "Pre-injection fluorescence in indocyanine green angiography," *Ophthalmology*, vol. 103, no. 11, pp. 1837–1845, 1996.

[7] H. M. Helb, P. C. Issa, M. Fleckenstein et al., "Clinical evaluation of simultaneous confocal scanning laser ophthalmoscopy imaging combined with high-resolution, spectral-domain optical coherence tomography," *Acta Ophthalmologica*, vol. 88, no. 8, pp. 842–849, 2010.

[8] F. Pichi, A. P. Ciardella, C. Torrazza et al., "A spectral-domain optical coherence tomography description of ND: YAG laser hyaloidotomy in premacular subhyaloid hemorrhage," *Retina*, vol. 32, no. 4, pp. 861–862, 2012.

[9] G. M. Lathrop, J. M. Lalouel, C. Julier, and J. Ott, "Strategies for multilocus linkage analysis in humans," *Proceedings of the National Academy of Sciences of the United States of America*, vol. 81, no. 11 I, pp. 3443–3446, 1984.

[10] G. M. Lathrop, J. M. Lalouel, C. Julier, and J. Ott, "Multilocus linkage analysis in humans: detection of linkage and estimation of recombination," *American Journal of Human Genetics*, vol. 37, no. 3, pp. 482–498, 1985.

[11] G. Querques, N. Leveziel, N. Benhamou, M. Voigt, G. Soubrane, and E. H. Souied, "Analysis of retinal flecks in fundus flavimaculatus using optical coherence tomography," *British Journal of Ophthalmology*, vol. 90, no. 9, pp. 1157–1162, 2006.

[12] K. W. Small, N. Udar, S. Yelchits et al., "North Carolina macular dystrophy (MCDR1) locus: a fine resolution genetic map and haplotype analysis," *Molecular Vision*, vol. 5, artile 38, 1999.

[13] K. W. Small, J. Weber, A. Roses, and P. Pericak-Vance, "North Carolina macular dystrophy (MCDR1): a review and refined mapping to 6q14–q16.2," *Ophthalmic Paediatrics and Genetics*, vol. 14, no. 4, pp. 143–150, 1993.

[14] K. W. Small, J. L. Weber, A. Roses, F. Lennon, J. M. Vance, and M. A. Pericak-Vance, "North Carolina macular dystrophy is assigned to chromosome 6," *Genomics*, vol. 13, no. 3, pp. 681–685, 1992.

[15] R. N. Khurana, X. Sun, E. Pearson et al., "A reappraisal of the clinical spectrum of North Carolina macular dystrophy," *Ophthalmology*, vol. 116, no. 10, pp. 1976–1983, 2009.

[16] H. R. Frank, M. B. Landers, R. J. Williams, and J. B. Sidbury, "A new dominant progressive foveal dystrophy," *American Journal of Ophthalmology*, vol. 78, no. 6, pp. 903–916, 1974.

[17] J. D. Gass, "Inherited macular disease," in *Stereoscopic Atlas of Macular Diseases: Diagnosis and Treatment*, J. D. Gass, Ed., vol. 1, pp. 98–99, Mosby, St. Louis, Mo, USA, 3rd edition, 1987.

[18] R. T. Smith, "Fundus autofluorescence patterns in stargardt disease over time," *Archives of Ophthalmology*, vol. 130, no. 10, pp. 1354–1355, 2012.

[19] C. A. Cukras, W. T. Wong, R. Caruso, D. Cunningham, W. Zein, and P. A. Sieving, "Centrifugal expansion of fundus autofluorescence patterns in Stargardt disease over time," *Archives of Ophthalmology*, vol. 130, no. 2, pp. 171–179, 2012.

[20] A. Giani, M. Pellegrini, E. Carini, A. Peroglio Deiro, F. Bottoni, and G. Staurenghi, "The dark atrophy with indocyanine green angiography in Stargardt disease," *Investigative Ophthalmology & Visual Science*, vol. 53, no. 7, pp. 3999–4004, 2012.

[21] S. Yzer, L. I. van den Born, M. N. Zonneveld et al., "Molecular and phenotypic analysis of a family with autosomal recessive cone-rod dystrophy and Stargardt disease," *Molecular Vision*, vol. 3, pp. 1568–1572, 2007.

[22] R. G. Coussa and E. I. Traboulsi, "Choroideremia: a review of general findings and pathogenesis," *Ophthalmic Genetics*, vol. 33, no. 2, pp. 57–65, 2012.

[23] A. Thobani, A. Anastasakis, and G. A. Fishman, "Microperimetry and OCT findings in female carriers of choroideremia," *Ophthalmic Genetics*, vol. 31, no. 4, pp. 235–239, 2010.

[24] M. N. Preising, E. Wegscheider, C. Friedburg, C. M. Poloschek, B. K. Wabbels, and B. Lorenz, "Fundus autofluorescence in carriers of choroideremia and correlation with electrophysiologic and psychophysical data," *Ophthalmology*, vol. 116, no. 6, pp. 1201.e2–1209.e2, 2009.

[25] K. Petrukhin, M. J. Koisti, B. Bakall et al., "Identification of the gene responsible for best macular dystrophy," *Nature Genetics*, vol. 19, no. 3, pp. 241–247, 1998.

[26] B. Wabbels, M. N. Preising, U. Kretschmann, A. Demmler, and B. Lorenz, "Genotype-phenotype correlation and longitudinal course in ten families with Best vitelliform macular dystrophy," *Graefe's Archive for Clinical and Experimental Ophthalmology*, vol. 244, no. 11, pp. 1453–1466, 2006.

[27] R. F. Spaide, K. Noble, A. Morgan, and K. B. Freund, "Vitelliform macular dystrophy," *Ophthalmology*, vol. 113, no. 8, pp. 1392–1400, 2006.

[28] B. Bakall, R. A. Radu, J. B. Stanton et al., "Enhanced accumulation of A2E in individuals homozygous or heterozygous for mutations in BEST1 (VMD2)," *Experimental Eye Research*, vol. 85, no. 1, pp. 34–43, 2007.

[29] A. D. Marmorstein, L. Y. Marmorstein, M. Rayborn, X. Wang, J. G. Hollyfield, and K. Petrukhin, "Bestrophin, the product of the Best vitelliform macular dystrophy gene (VMD2), localizes to the basolateral plasma membrane of the retinal pigment epithelium," *Proceedings of the National Academy of Sciences of the United States of America*, vol. 97, no. 23, pp. 12758–12763, 2000.

[30] D. C. Hood, A. V. Cideciyan, A. J. Roman, and S. G. Jacobson, "Enhanced S cone syndrome: svidence for an abnormally large number of S cones," *Vision Research*, vol. 35, no. 10, pp. 1473–1481, 1995.

[31] U. Kellner, E. Zrenner, B. Sadowski, and M. H. Foerster, "Enhanced S cone sensitivity syndrome: long-term follow-up, electrophysiological and psychophysical findings," *Clinical Vision Sciences*, vol. 8, no. 5, pp. 425–434, 1993.

[32] N. B. Haider, S. G. Jacobson, A. V. Cideciyan et al., "Mutation of a nuclear receptor gene, NR2E3, causes enhanced S cone syndrome, a disorder of retinal cell fate," *Nature Genetics*, vol. 24, no. 2, pp. 127–131, 2000.

[33] H. Yamamoto, A. Simon, U. Eriksson, E. Harris, E. L. Berson, and T. P. Dryja, "Mutations in the gene encoding 11-cis retinol dehydrogenase cause delayed dark adaptation and fundus albipunctatus," *Nature Genetics*, vol. 22, no. 2, pp. 188–191, 1999.

[34] N. K. Wang, H. F. Fine, S. Chang et al., "Cellular origin of fundus autofluorescence in patients and mice with a defective NR2E3 gene," *British Journal of Ophthalmology*, vol. 93, no. 9, pp. 1234–1240, 2009.

[35] P. Schatz, M. Preising, B. Lorenz et al., "Lack of autofluorescence in fundus albipunctatus associated with mutations in RDH5," *Retina*, vol. 30, no. 10, pp. 1704–1713, 2010.

[36] M. A. Genead, G. A. Fishman, and M. Lindeman, "Spectral-domain optical coherence tomography and fundus autofluorescence characteristics in patients with fundus albipunctatus and retinitis punctata albescens," *Ophthalmic Genetics*, vol. 31, no. 2, pp. 66–72, 2010.

[37] G. Querques, P. Carrillo, L. Querques, A. V. Bux, M. V. del Curatolo, and N. delle Noci, "High-definition optical coherence tomographic visualization of photoreceptor layer and retinal flecks in fundus albipunctatus associated with cone dystrophy," *Archives of Ophthalmology*, vol. 127, no. 5, pp. 703–706, 2009.

Hindawi Publishing Corporation
Journal of Ophthalmology
Volume 2013, Article ID 309192, 4 pages
http://dx.doi.org/10.1155/2013/309192

Clinical Study

Autofluorescence Images with Carl Zeiss versus Topcon Eye Fundus Camera: A Comparative Study

Juan M. Muñoz,[1,2] Rosa M. Coco,[1] M. Rosa Sanabria,[1,3] Ruben Cuadrado,[1] and Eduardo Blanco[1]

[1] *Instituto de Oftalmobiologia Aplicada (IOBA), Universidad de Valladolid, Spain*
[2] *Consultorio 225, Consultorios América, Vía España, Panamá, Panama*
[3] *Complejo Asistencial de Palencia, Spain*

Correspondence should be addressed to Juan M. Muñoz; j_m_munoz@yahoo.com

Received 18 January 2013; Revised 1 April 2013; Accepted 2 April 2013

Academic Editor: Atsushi Hayashi

Purpose. To compare the autofluorescence images of the Zeiss versus Topcon eye fundus cameras and design an objective way to quantify it. *Procedures*. The IMAGEJ software was used to determine the gray level corresponding to the darkest veins and the peripapillary ring (thresholds), the level of white of the brightest perifoveal area, their difference (contrast level), and the suprathreshold area for each photograph. *Results*. Carl Zeiss has higher contrast values than Topcon. The Topcon contrast presented a crest with further decline as the suprathreshold area continued to increase. On the contrary, the Zeiss profile did not decline in contrast. *Conclusions and Message*. The Carl Zeiss camera showed superior contrast ability over the Topcon when performing autofluorescence imaging. We set objective parameters to compare fundus cameras FAF images. These parameters could be the base to objectively measure and determine changes and realize followup to areas of hyper- or hypofluorescence.

1. Introduction

Fundus autofluorescence (FAF) imaging is a noninvasive imaging method which provides additional information not obtainable with other imaging techniques [1], or ordinary fundus examination [2]. FAF became recently available in the last decade with the introduction of confocal laser scanning ophthalmoscopes, by using an exciting wavelength of 488 nm and detecting the light emitted above 500 nm [3].

There are several tissues having autofluorescent properties within the eye, such as the cornea, the lens, the retinal pigment epithelium (RPE), the uveal melanocytes, and the scleral collagen, but the main source of fundus autofluorescence is lipofuscin localized at the level of the RPE [4, 5]. Lipofuscin is intrinsic retinoid fluorophores, toxic coproduct of the photoreceptors, that accumulates in the lysosomes of the RPE, possibly due to incomplete degradation of photoreceptor outer segments. The concept of FAF relies on natural fluorescence occurring from the retinal layers, providing an indicator of the RPE monolayer health. FAF imaging may identify first signs of retinal diseases before they are evident. Low pixel values (dark) illustrate low intensities and high pixel values (bright) high intensities, respectively. The optic nerve head and retinal vessels typically appear dark as they obscure the normal RPE FAF underlying [6]. Besides the intensity of FAF ($\log[F(\text{end})]$) is lowest at the center of the fovea and increased gradually toward the periphery within a 270-pixel square [7]. Moreover, FAF can be correlated with specific patterns identified by autofluorescence and can also be used as a monitoring tool after therapeutic procedures as retinal detachment, macular surgery, or laser treatment [3, 8–11].

The available data on FAF imaging suggest that it is possible to relatively differentiate between normal and abnormal FAF intensities over certain regions of the retina in individual patients. However, little has been published regarding FAF imaging methods able to objectively quantify alterations in the magnitude and localization of the FAF intensity in a single patient or between patients [1, 8]. In addition, although the photopigment has been assessed in Scanning Laser Ophthalmoscopy (SLO) pictures by using

the fluorescence optical density difference (fODD) [12], no quantitative models have been described, to quantify and compare autofluorescence images from eye fundus cameras. Even though the images of SLO are always focused and seem to provide the clinician a better resolution, eye fundus cameras are more widespread and available in many ophthalmologic centers.

Finally, the contrast might be considered as the main indicator of quality of a gray photograph and refers to the ability to capture dark and bright zones at the same time [13]. It depends on multiple factors including reflectivity of the optic system and the illuminance [14]. The purpose of our study was to compare the quality of contrast imaging FAF between the Zeiss and Topcon camera. In order to do that, we also developed a quantitative method to compare the FAF by comparing the contrast levels of the two images, determining areas to be used as reference and thresholds, calculating suprathreshold areas of both cameras, and establishing a correlation between contrast and suprathreshold areas.

2. Methods

In our study, we took FAF photographs to every patient sent to the IOBA (a referral center) from the CAPA, who fulfilled the following criteria: (1) eyes without retinal detachment, (2) transparent media (cornea, anterior chamber, lens, and vitreous), (3) good cooperation to allow the capture of the photographs, and (4) proper health condition to allow the photograph capture.

We compared the Topcon TRC-50IX with a Kodak Megaplus 1.4i camera and the Zeiss FF 450 Plus IR with Visupac 4.1, and a Kodak Megaplus 1.6 camera (available in IOBA and CAPA, resp.). The Carl Zeiss used an exciter filter of 510–580 nm and a barrier filter of 650–735 nm, while the Topcon used an exciter filter of 500 to 610 nm and a barrier filter of 675 to 715 nm. All the photographs were taken by certified eye fundus photographers, including 50° of the posterior pole, centered on the fovea.

We used the IMAGEJ software from the National Health Institute of the United States, specially designed for images analysis. The software is able to determine the gray level of any point within the picture and to locate it in a scale of 256 gray levels, where 0 is absolute black, and 255 is absolute white. The software is also able to calculate a suprathreshold area over a gray level within a photograph. The images were brought to the same size for the comparison. All the 50[a] images were resized 1280 × 1024 pixels before being processed.

To determine the contrast (what we called "Δ"), we measured the gray level of 3 points within the darkest peripapillary ring, 3 points in the darkest areas of the biggest veins, and 3 points in the brightest perifoveal area. For each photograph, we estimated 2 "Δ" values. The first one was the difference between the average of the brightest perifoveal points and the average of the darkest points of the veins. The second was the difference between the average of the brightest perifoveal points and the average of the darkest peripapillary points. When comparing the Δ values between different areas, we used the formula: $t = \overline{x}T - \overline{x}C/\mathrm{sq}(\mathrm{var}T/nT + \mathrm{var}C/nC)$ where alfa = 0.05, and degrees of freedom = 24. We also calculated the brighter area of the photographs over the corresponding average of the veins gray level and over the corresponding average of the peripapillary ring area.

For the statistical processing, we performed the Student's t-test for two independent samples assuming unequal variances. We used the Microsoft Excel to calculate regression models to find out any correlation between the contrast levels and the suprathreshold areas in the photographs.

The informed consent was obtained. The researchers have no commercial interests in this study. This study followed the tenets of Helsinki.

3. Results

Thirteen autofluorescence images from seven patients were included. One eye of one of the patients was excluded because of media opacity.

When comparing the Δ values between veins and the perifoveal area using the formula given above, we obtained a $t = 2.86$, for a P value = 0.006, indicating statistical differences, with higher contrast values for the Carl Zeiss camera. When comparing the Δ values between the peripapillary ring and the perifoveal area, we found that $t = 3.44$, for P value = 0.001, indicating a significant difference and a higher contrast for the Carl Zeiss camera too.

For the visible area over the veins threshold, we found no difference between the two cameras ($t = 0.759$, P value = 0.23), but we did find differences for the visible area over the peripapillary ring threshold between the two cameras ($t = 2.60$, $P = 0.01$). The largest suprathreshold area corresponded to the Topcon, which subjectively showed a better defined mask too (Figure 1).

These findings made us consider a possible correlation between the Δ values for contrast and the suprathreshold areas found in the autofluorescence photographs. The correlation graphs appeared to follow 2nd order polinomic equations, as showed in Figures 2 and 3.

For the brighter area over the veins threshold, we found no difference between the two cameras ($t = 0.759$, P value > 0.05). We did find difference for the brighter area over the peripapillary ring threshold between the two cameras ($t = 2.60 > 2.064$, $P < 0.05$). The largest suprathreshold area corresponded to the Topcon. The Topcon camera subjectively showed a better defined mask (Figure 1).

These findings made us consider a possible correlation between the "Δ" values for contrast and the suprathreshold areas found in the autofluorescence photographs. The correlation graphs appeared to follow the 2nd order polinomic equations, as showed in Figures 2 and 3.

4. Discussion

The contrast value measured with the J Image software is an objective form to estimate the ability of a camera, to accurately capture an image, by reproducing details within the brightest and the darkest sides of a grayscale at the same time [13, 14].

We found that the peripapillary ring is closer to an absolute black value within the grayscale, and we think it

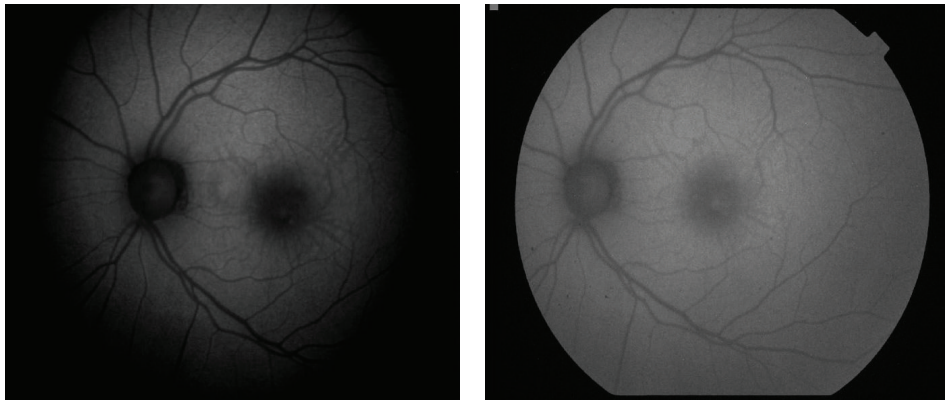

(a) (b)

Figure 1: Macular star photographed with the Carl Zeiss camera (a) and the Topcon camera (b). Notice more marked difference between light gray and dark gray for the Carl Zeiss and the better defined mask for the Topcon.

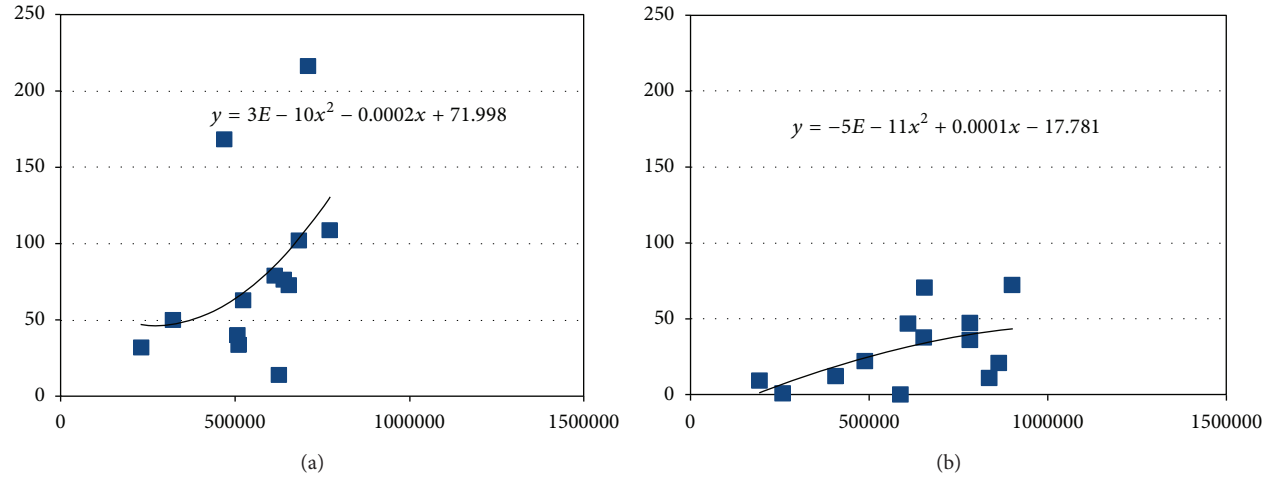

(a) (b)

Figure 2: Correlation between the contrast (D value) in the y-axis and the area over the veins threshold (pixels) in the x-axis, for the Carl Zeiss (a) and the Topcon camera (b).

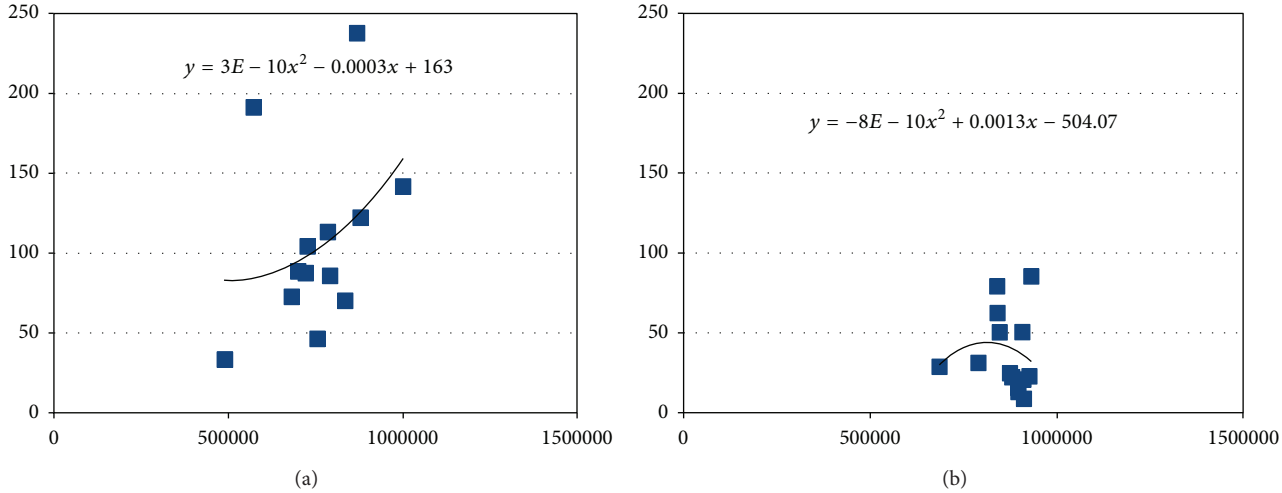

(a) (b)

Figure 3: Correlation between the contrast (D value) in the y-axis and the area over the peripapillary ring threshold (pixels) in the x-axis, for the Carl Zeiss (a) and the Topcon camera (b).

is probably because the veins are narrow and closer to the brightest area around the fovea.

The differences in contrast values could be due to the illumination, reflectivity, and sensor capability. These factors can be influenced by the quality of the optical system, and of the sensor *per se*, but also by the software of any camera [15]. The contrast or dynamic range refers to the amount of grayscale in an image. For digital imaging, this describes the system's ability to reproduce tonal information by the difference between the lightest light and darkest dark of an image [16].

In the graphics of contrast versus suprathreshold area, we noticed a similar behavior of the curves for the two cameras. Nevertheless, the Microsoft Excel software estimated somehow similar equations for the Carl Zeiss. Both curves followed a polinomic behavior, where the suprathreshold area increased with the increase in contrast. Unlike the Carl Zeiss, the Topcon curves showed increasing contrast with the increase in the suprathreshold area, until contrast values ("Δ") of around 45, where they showed a crest with further decline in the contrast as the area continued to increase. These findings suggest that the image quality worsen progressively at this point, even though the suprathreshold area continued to increase. The mask was better defined with the Topcon camera in all points.

5. Conclusions

The Carl Zeiss camera showed higher contrast values over the Topcon for autofluorescence imaging. This could be due to its Kodak Megaplus sensor 1.6, its illumination, optical system, quality of the filters, or capability of the software used. The precise reason is beyond the objective of our study.

Our study established objective parameters as cornerstones for the quantification of the autofluorescence imaging with eye fundus cameras. These parameters could also be used to objectively measure and determine changes in areas of hyper- or hypofluorescence and for their followup along time, every time a normal variability has been defined with a larger series of photographs to a given eye in a precise moment.

References

[1] S. Schmitz-Valckenberg, M. Fleckenstein, H. P. N. Scholl, and F. G. Holz, "Fundus autofluorescence and progression of age-related macular degeneration," *Survey of Ophthalmology*, vol. 54, no. 1, pp. 96–117, 2009.

[2] K. Shiraki, T. Kohno, M. Moriwaki, and N. Yanagihara, "Fundus autofluorescence in patients with pseudoxanthoma elasticum," *International Ophthalmology*, vol. 24, no. 5, pp. 243–248, 2001.

[3] C. Framme, J. Roider, H. Sachs1 et al., "Noninvasive imaging and monitoring of retinal pigment epithelium patterns using fundus autofluorescence—review," *Current Medical Imaging Reviews*, vol. 1, pp. 89–103, 2005.

[4] C. L. Shields, C. Pirondini, C. Bianciotto, S. A. Harmon, and J. A. Shields, "Autofluorescence of congenital hypertrophy of the retinal pigment epithelium," *Retina*, vol. 27, no. 8, pp. 1097–1100, 2007.

[5] R. F. Spaide and J. M. Klancnik, "Fundus autofluorescence and central serous chorioretinopathy," *Ophthalmology*, vol. 112, no. 5, pp. 825–833, 2005.

[6] A. Hassenstein and C. H. Meyer, "Clinical use and research applications of Heidelberg retinal angiography and spectral-domain optical coherence tomography—a review," *Clinical and Experimental Ophthalmology*, vol. 37, no. 1, pp. 130–143, 2009.

[7] T. Sekiryu, T. Iida, I. Maruko, and M. Horiguchi, "Clinical application of autofluorescence densitometry with a scanning laser ophthalmoscope," *Investigative Ophthalmology and Visual Science*, vol. 50, no. 6, pp. 2994–3002, 2009.

[8] V. Vaclavik, S. Vujosevic, S. S. Dandekar, C. Bunce, T. Peto, and A. C. Bird, "Autofluorescence imaging in age-related macular degeneration complicated by choroidal neovascularization. A prospective study," *Ophthalmology*, vol. 115, no. 2, pp. 342–346, 2008.

[9] A. von Rückmann, F. Fitzke, and A. Bird, "*In vivo* fundus autofluorescence in macular dystrophies," *Archives of Ophthalmology*, vol. 115, p. 611, 1997.

[10] C. Shiragami, F. Shiraga, E. Nitta, K. Fukuda, and H. Yamaji, "Correlation of increased fundus autofluorescence signals at closed macula with visual prognosis after successful macular hole surgery," *Retina*, vol. 32, no. 2, pp. 281–288, 2012.

[11] C. Shiragami, F. Shiraga, H. Yamaji et al., "Unintentional displacement of the retina after standard vitrectomy for rhegmatogenous retinal detachment," *Ophthalmology*, vol. 117, no. 1, pp. 86.e1–92.e1, 2010.

[12] S. M. Waldstein, D. Hickey, I. Mahmud et al., "Two-wavelength fundus autofluorescence and macular pigment optical density imaging in diabetic macular oedema," *Eye*, vol. 26, no. 8, pp. 1078–1085, 1997.

[13] W. Kim, J. You, and J. Jeong, "Contrast enhancement using histogram equalization based on logarithmic mapping," *Optical Engineering*, vol. 51, no. 6, Article ID 067002, 2012.

[14] P. C. Issa, M. S. Singh, D. M. Lipinski et al., "Optimization of in vivo confocal autofluorescence imaging of the ocular fundus in mice and its application to models of human retinal degeneration," *Investigative Ophthalmology & Visual Science*, vol. 53, no. 2, pp. 1066–1075, 2012.

[15] R. Huang, N. Sang, D. Luo, and X. Tong, "Enhancing low-contrast image by separately processing illuminance and reflectance," in *Visual Information Processing XIX*, vol. 7701 of *Proceedings of SPIE*, 2010.

[16] I. Indrajit and B. Verma, "Digital imaging in radiology practice: an introduction to few fundamental concepts," *Indian Journal of Radiology and Imaging*, vol. 17, no. 4, pp. 230–236, 2007.

Hindawi Publishing Corporation
Journal of Ophthalmology
Volume 2013, Article ID 518170, 7 pages
http://dx.doi.org/10.1155/2013/518170

Review Article

Photoreceptor Impairment and Restoration on Optical Coherence Tomographic Image

Yoshinori Mitamura,[1] Sayaka Mitamura-Aizawa,[1] Takashi Katome,[1] Takeshi Naito,[1] Akira Hagiwara,[2] Ken Kumagai,[2] and Shuichi Yamamoto[2]

[1] *Department of Ophthalmology, Institute of Health Biosciences, The University of Tokushima Graduate School, Tokushima 770-8503, Japan*
[2] *Department of Ophthalmology and Visual Science, Chiba University Graduate School of Medicine, Chiba, Japan*

Correspondence should be addressed to Yoshinori Mitamura; ymitaymitaymita@yahoo.co.jp

Received 8 January 2013; Accepted 17 March 2013

Academic Editor: Masanori Hangai

With recent development of spectral-domain optical coherence tomography (SD-OCT), the pathological changes of retina can be observed in much greater detail. SD-OCT clearly delineates three highly reflective lines in the outer retina, which are external limiting membrane (ELM), photoreceptor inner and outer segment (IS/OS) junction, and cone outer segment tips (COST) in order from inside. These lines can serve as hallmarks for the evaluation of photoreceptor condition. In retinitis pigmentosa (RP) leading to photoreceptor degeneration, the ELM, IS/OS, and COST lines are shortened with the progression of the disease. In addition, shortening of the ELM, IS/OS and COST lines is significantly associated with each other. The line length is longest in the ELM, followed by the IS/OS, and COST, suggesting that retinal layer becomes disorganized first at the COST, followed by the IS/OS and finally the ELM. This finding is consistent with the previous report that the earliest histopathological change in RP is a shortening of the photoreceptor outer segments. On the other hand, retinal layer becomes restored first at the ELM, followed by the IS/OS and finally the COST after macular hole surgery. There may be a directionality of photoreceptor impairment or restoration on optical coherence tomographic image.

1. Advancement of Optical Coherence Tomography Instrument

Optical coherence tomography (OCT) is a well-established method of examining the retinal architecture *in vivo*. After the introduction of OCT, *in vivo* imaging of the retina of various retinal diseases came true. In particular, the ease with which these images can be acquired considerably changed the diagnostic strategy used by ophthalmologists [1].

With most recent development of spectral-domain OCT (SD-OCT), the pathological changes of retina can be observed in much greater detail. SD-OCT technology uses low-coherence interferometry to detect light echoes, relying on a spectrometer and high-speed camera and based on the mathematical premise of the Fourier transformation [2]. Because application of the Fourier transformation has the effect of measuring all echoes of light simultaneously, as compared with sequentially in the case of time-domain OCT (TD-OCT), SD-OCT significantly increases the amount of data acquired in each session, resulting in a significant reduction of motion artifacts and an increased signal-to-noise ratio compared with TD-OCT. The axial resolution of TD-OCT was 10–20 μm. SD-OCT (5 to 6 μm of axial resolution) has improved the ability to detect intraretinal microstructures and to identify pathological changes in the retinal architecture in various diseases.

SD-OCT clearly delineates three highly reflective lines in the outer retina, which are external limiting membrane (ELM), photoreceptor inner and outer segment (IS/OS) junctions, and cone outer segment tips (COST) in order from inside. These lines can serve as hallmarks for the evaluation of photoreceptor condition [3]. In this review, we summarize the changes of these three lines on the SD-OCT images due to the photoreceptor impairment and restoration.

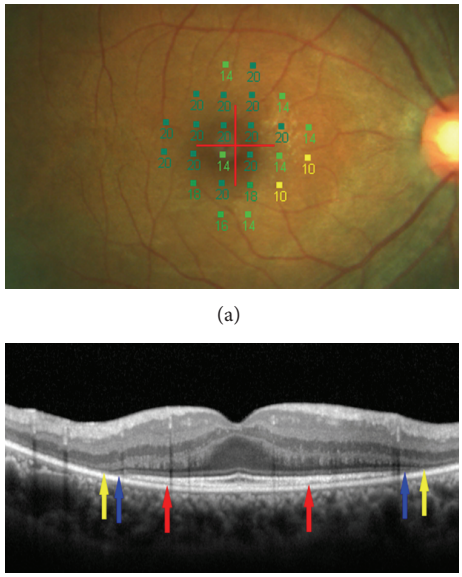

(a)

(b)

Figure 1: Microperimetric map and spectral-domain optical coherence tomographic (SD-OCT) image of an eye with retinitis pigmentosa (42-year-old woman). (a) Microperimetric map image. A total of 24 stimulus locations covering the central 10° field were tested. The mean retinal sensitivity at the 24 locations is 17.3 dB. The best corrected visual acuity was 1.0. (b) SD-OCT image of a vertical scan. In addition to photoreceptor inner/outer segment (IS/OS) junction line, the external limiting membrane (ELM) and cone outer segment tips (COST) lines are clearly seen on the SD-OCT image. Red arrows indicate end points of the COST line. Blue arrows indicate end points of the IS/OS line and yellow arrows end points of the ELM line. The lengths of the COST, IS/OS, and ELM lines were computed at 2272, 4629, and 4930 μm, respectively. Note that the line length was the longest in the ELM, followed by the IS/OS and COST. The direction of photoreceptor impairment is from outside toward inside.

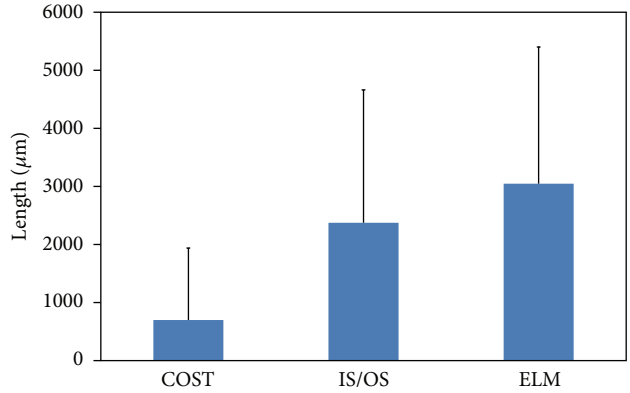

Figure 2: Mean lengths of the cone outer segment tips (COST), photoreceptor inner and outer segment (IS/OS) junction, and external limiting membrane (ELM) lines in 133 eyes with retinitis pigmentosa. The ELM length was significantly longer than the IS/OS or COST length, and the IS/OS length was significantly longer than the COST length (all $P < 0.0001$). Error bars represent one standard deviation from the mean.

2. Photoreceptor Impairment on Optical Coherence Tomographic Image

Retinitis pigmentosa (RP) is a slowly progressive inherited retinal disease, and the patients experience reduced visual function because of the degeneration of the photoreceptors and the retinal pigment epithelium (RPE). The loss of the central photoreceptors reduces central vision at the end stage of the disease. In OCT, retinal edema or hemorrhage may weaken the signal intensity of the outer retinal layers, making it difficult to detect the reflections from the ELM, IS/OS, or COST [4]. In Japanese RP patients, however, it has been reported that macular abnormalities such as cystoids macular edema or epiretinal membrane were detected by OCT in only 7.4% of 622 eyes with RP [5]. Therefore, RP is a good candidate for image assessment of the photoreceptor impairment on the OCT images.

In RP patients, the IS/OS line disappeared from peripheral part toward fovea on the OCT images with the progression of the disease. Therefore, measuring the length of the residual IS/OS line can be useful in estimating the residual central visual function in RP patients. Using TD-OCT, it has been reported that the length or the presence of the IS/OS line was significantly correlated with visual acuity in 300 eyes with RP [6]. In addition, the length of the IS/OS line was highly correlated with the retinal sensitivity in RP patients [7]. It has also been reported that the length of the IS/OS line decreased with the progression of RP during the follow-up period of more than 2 years [8]. Shortening of the IS/OS line was accompanied by a decrease in retinal sensitivity and a worsening of the visual acuity. The decrease in IS/OS length was significantly correlated with the decrease in retinal sensitivity and visual acuity [8]. These results indicate that a progressive IS/OS shortening may reflect morphological changes of the photoreceptors and worsening of visual function in the progression of RP. Thus, the IS/OS line may be an important parameter to monitor in RP patients.

Using SD-OCT, a recent study reported the results of examination of 133 patients with RP [9]. In this study, the lengths of the residual ELM, IS/OS, and COST lines were measured on SD-OCT images (Figure 1). The Micro Perimeter-1 (MP-1) (Nidek, Gamagori, Japan) was used to determine the mean retinal sensitivity at 24 locations covering the central 10° (Figure 1). The ELM length was significantly longer than the IS/OS or COST length, and the IS/OS length was significantly longer than the COST length (all $P < 0.0001$, Figure 2). In all subject eyes, the length was longest in the ELM, followed by the IS/OS and COST. The correlations among the ELM, IS/OS, and COST lengths were extremely significant (all $P < 0.0001$, Figure 3). The ELM, IS/OS, and COST lengths were significantly correlated with the mean retinal sensitivity and the visual acuity (all $P < 0.01$, Figure 4).

This study showed that the ELM, IS/OS, and COST lengths were highly correlated with each other and were significantly correlated with visual function. In each eye of

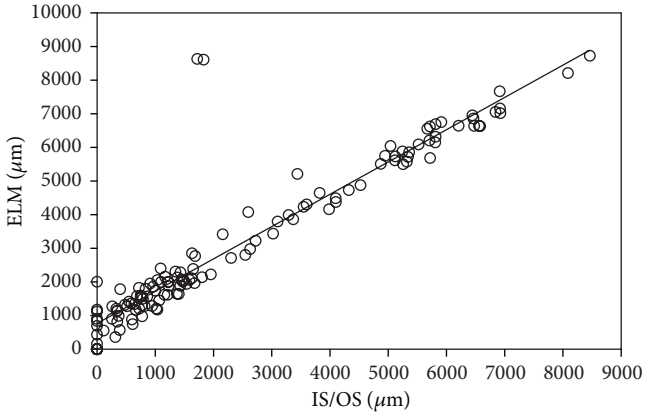

Figure 3: Correlation between the lengths of the photoreceptor inner/outer segment (IS/OS) junction and the external limiting membrane (ELM) lines in 133 eyes with retinitis pigmentosa. There is a significant positive correlation between the lengths of the IS/OS and ELM lines ($r = 0.933$, $P < 0.0001$). The solid line represents the linear regression curve ($y = 768.13 + 0.96x$).

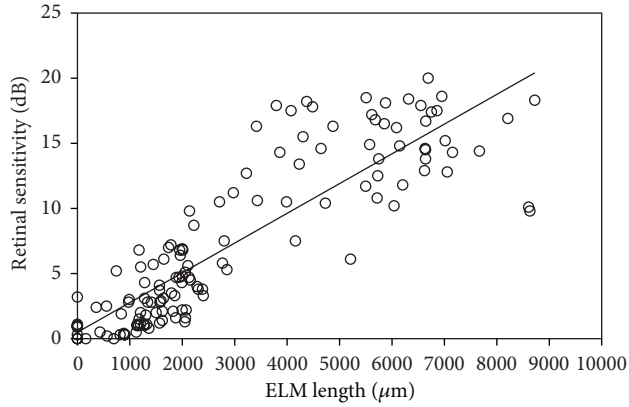

Figure 4: Correlation between the length of the external limiting membrane (ELM) line and the mean retinal sensitivity in 133 eyes with retinitis pigmentosa. There is a significant positive correlation between the length of the ELM line and the retinal sensitivity ($r = 0.868$, $P < 0.0001$). The solid line represents the linear regression curve ($y = 0.488 + 0.002x$).

all subjects, the length was the longest in the ELM, followed by the IS/OS and COST lines. These findings suggested that the shortening of the ELM, IS/OS, and COST lines is associated with each other and that retinal layer may become disorganized first at the COST line, followed by the IS/OS line and finally the ELM line. Wakabayashi et al. [10] also reported that the ELM length was significantly longer than the IS/OS length in RP patients. To exactly determine the time course of the changes in the ELM, IS/OS, and COST lines in RP patients, however, further follow-up longitudinal studies will be required.

Previous pathological studies of RP indicated that the earliest histopathological change in the rods is shortening of their outer segments, which can be visualized by immunocytochemistry using antirhodopsin [11]. The connecting cilium is a narrow stalk that joins the inner and outer segments of rods and cones. Several reports indicated that connecting cilia may be abnormal in RP patients [12, 13]. A structural or functional defect in the connecting cilium could result in decreased transport of newly synthesized proteins from the inner to the outer segment, resulting in the outer segment shortening and dysfunction that are characteristic of RP. Rod cell death in RP retinas is usually accompanied by changes in the neighboring cones, including outer segment shortening, cytoplasmic densification, axonal elongation, and, ultimately, cone cell death [14]. When all rods and most of the cones have died, the macula usually retains a monolayer of cone somata with very short or absent outer segments [14]. These pathological changes in RP are consistent with the OCT findings that retinal layer becomes disorganized first at the COST line, followed by the IS/OS line and finally the ELM line.

As for acute zonal occult outer retinopathy (AZOOR), Tsunoda et al. [15] reported that the COST line may be an early indicator of photoreceptor dysfunction in AZOOR. In their AZOOR cases, the COST line was always absent in the region of IS/OS abnormalities. Therefore, the authors concluded that the abnormality of the COST line may precede that of the IS/OS junction. In the region with the COST line abnormality in their AZOOR cases, the IS/OS junction was clearly observed, but the amplitude in focal macular electroretinograms and the retinal sensitivity were markedly reduced. Thus, the authors suggested that the photoreceptor dysfunction could be initially reflected by an absence or indistinctness of the COST line. However, care should be taken in the evaluation of the COST line because visibility of the COST line is dependent on the intensity and direction of the laser light that reaches the photoreceptor layer [16]. As an indicator of early cone photoreceptor dysfunction, the authors also found the foveal bulge which indicates a domelike appearance of the IS/OS junction due to an elongated cone outer segment at the fovea [15]. The foveal bulge could not be detected in their AZOOR cases with COST line abnormality and continuous IS/OS.

With respect to other retinal degenerative diseases, Lazow et al. [17] examined the structural changes across the transition zone between relatively normal retina and severely affected retina in choroideremia (CHM) and the Stargardt disease (STGD), and compared these to the transition zone in RP using SD-OCT. The ELM disappeared in a more affected location than did the IS/OS junction in all CHM and STGD patients, and these findings were similar to those in RP. These findings suggested that retinal layer may become disorganized at the IS/OS line, followed by the ELM line not only in RP but also in CHM and STGD. However, there were qualitative differences in the appearance of the transition zones. The distance between the disappearance point of the IS/OS line and the ELM line was significantly shorter in CHM and STGD, as compared with that in RP. In other words, the disappearances of the IS/OS and ELM lines were gradual (shallower slope) in RP, yet were nearly vertical (steeper slope) in CHM and STGD. Thus, the disappearances of

the IS/OS junction and ELM were much more abrupt in CHM and STGD than in RP.

As for retinal impairment due to retinal detachment (RD), Wakabayashi et al. [18] evaluated foveal microstructural changes in eyes with anatomically successful repair of rhegmatogenous RDs using SD-OCT. In their study, no eyes had a disrupted ELM with an intact IS/OS junction, suggesting that mechanical splitting of the photoreceptor outer segments and RPE adhesion in RDs initially damages the photoreceptor outer segment layer and then causes degenerative changes that reach the photoreceptor cell bodies. As for evidence supporting this suggestion, several experimental studies have reported that the degenerated photoreceptor outer segment and the decreased outer segment length occur immediately after RDs [19, 20]. Apoptotic changes in the photoreceptor cells occur soon after detachment [21], followed by progressive loss of photoreceptors in eyes with long-standing RDs [22].

With respect to epiretinal membrane (ERM), Shimozono et al. [23] studied 50 eyes with idiopathic ERM using SD-OCT. There were no eyes with ELM disruption. The IS/OS junction also retained its continuity in all cases, while the COST line was disrupted in 48%. The authors speculated that the tractional force generated by ERM can alter the interface between the outer segment tips and the RPE without severely damaging the outer segment itself or photoreceptor cell bodies. In contrast, in more vision-threatening diseases such as age-related macular degeneration, the COST line is almost totally deteriorated, and the IS/OS junction, and even the ELM are disrupted in many cases [24]. Thus, there should be a hierarchy of vulnerability among the 3 lines; the COST line, the IS/OS junction and the ELM can be disrupted when mild, moderate, and severe photoreceptor damage, respectively, is caused [23].

3. Photoreceptor Restoration on Optical Coherence Tomographic Image

For the image assessment of the photoreceptor restoration on the OCT images, a lot of studies using OCT have reported on the relationship between the restoration of IS/OS junction and the recovery of the visual acuity after successful macular hole (MH) closure [25–30]. Using TD-OCT, it has been reported that the presence of the IS/OS line on the OCT images is correlated with the recovery of good vision after MH surgery and is essential for normal visual function [28].

After development of SD-OCT, SD-OCT images were analyzed in terms of the IS/OS junction and the ELM after idiopathic MH surgery. Ooka et al. [25] studied 43 eyes before and 1, 3, and 6 months after MH surgery. After MH surgery, the IS/OS or ELM line is restored from perifoveal region toward center of the closed MH on the OCT images. Therefore, measuring the length of defect in the IS/OS or ELM line can be useful in estimating the retinal restoration after MH surgery. The results of this study indicated that the length of the IS/OS junction defect was significantly correlated with the length of the ELM defect at all preoperative and postoperative times and that the restoration of the ELM was earlier than that of the IS/OS junction at all times and in all eyes. None of the eyes had a complete restoration of the IS/OS junction without a complete recovery of the ELM. These findings suggest that the restoration of the ELM is closely associated with that of the IS/OS junction, and the integrity of the ELM is necessary for the restoration of the IS/OS junction. At all postoperative times, the lengths of both the IS/OS and ELM defects were significantly correlated with both the visual acuity and the foveal sensitivity measured using MP-1. The restoration of the IS/OS junction and the ELM may reflect the morphological and functional recovery of the foveal photoreceptors in surgically closed MHs.

With respect to the COST line, it was reported that distinct COST line was first seen at 6 months after MH surgery [30]. On the other hand, distinct ELM and IS/OS lines were reported to be first seen at 1 month after surgery [30]. Itoh et al. [26] studied 51 eyes with MH before and 1, 3, 6, 9, and 12 months after MH surgery. The postoperative mean length of COST line defect progressively decreased, and the appearance of the COST line recovery began at the perifoveal region and progressed toward the center of the closed MH. The length of the COST line defect was significantly correlated with the visual acuity at 1, 3, 6, 9, and 12 months postoperatively. The recovered COST line was observed only in eyes with the intact IS/OS junction and ELM line. The length of COST line defect was significantly longer than that of the IS/OS or ELM line defect (both $P < 0.01$). Taken together with the results of the previous study [25], retinal layer becomes restored first at the ELM, followed by the IS/OS and finally the COST after MH surgery (Figure 5).

With respect to retinal restoration after ERM surgery, Shimozono et al. [23] studied 50 eyes that underwent vitrectomy for idiopathic ERM. There were no eyes with ELM disruption preoperatively and postoperatively. At baseline, the IS/OS junction retained its continuity in all cases, while the COST line was disrupted in 48%. The disruption of the IS/OS junction and the COST lines temporarily increased at 1 month postoperatively and decreased to near the baseline level thereafter. Postoperatively, defect lengths of IS/OS and COST lines were significantly correlated with the visual acuity.

As for retinal restoration after RD surgery, Wakabayashi et al. [18] evaluated foveal microstructural changes in eyes with anatomically successful repair of rhegmatogenous RDs using SD-OCT. In preoperative macula-off eyes, the postoperative visual acuity was significantly correlated with the integrity of the photoreceptor IS/OS and ELM lines detected by SD-OCT postoperatively. During the postoperative follow-up period, the IS/OS junction became restored in 64% of the eyes with the disrupted IS/OS junction and the continuous ELM line at the postoperative initial examination. In any eyes with the disrupted IS/OS and ELM at the initial examination, the photoreceptor layer did not become completely restored during the follow-up period. Thus, the authors concluded that the postoperative preservation of the ELM may predict the subsequent restoration of the photoreceptor layer in RD patients [18].

Regarding the histopathological findings of the detached retina after retinal reattachment, previous experimental

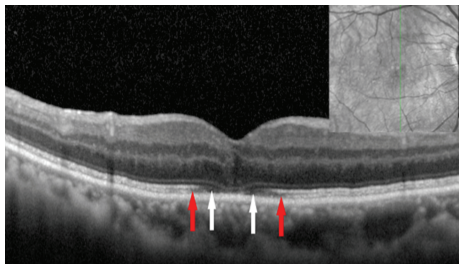

Figure 5: Spectral-domain optical coherence tomographic (SD-OCT) image of an eye 3 weeks after macular hole repair (72-year-old woman). SD-OCT image of a vertical scan was obtained. In addition to photoreceptor inner/outer segment (IS/OS) junction line, the external limiting membrane (ELM) and cone outer segment tips (COST) lines are clearly seen on the SD-OCT image. Red arrows indicate end points of the COST line. White arrows indicate end points of the IS/OS line. The ELM line has been almost restored. Note that the defect length was longest in the COST, followed by the IS/OS and ELM. The direction of photoreceptor restoration is from inside toward outside.

studies have proposed that atrophy of the photoreceptors occurring soon after retinal reattachment may be irreversible in eyes with extended period of RD [19, 20, 22, 31]. However, the atrophy can stop or reverse in eyes with short time period of RD [19, 20, 22, 31]. Guérin et al. [19] investigated the recovery process of photoreceptor outer segments after retinal reattachment using the animal model of RD. RD leads to a reduction in photoreceptor outer segment absolute length. Increasing time of retinal reattachment is positively correlated with an increase in outer segment absolute length. Rod and cone outer segments regained approximately 40% of their control lengths after a 2-week reattachment period. By 30 days of reattachment, rod outer segments had regained 72% of their normal length, and cone outer segments had regained approximately 48%. After 150 days of reattachment, photoreceptor outer segment mean length was not statistically different from control areas. This histopathological finding of increase in the photoreceptor outer segment length after retinal reattachment suggested the direction of photoreceptor restoration from inside toward outside, being consistent with the SD-OCT findings after the repair of RD [18].

The process of the photoreceptor restoration after MH or RD surgery seems to be exact opposite of the process of photoreceptor impairment in RP or other retinal degenerative diseases. It is known that the photoreceptors continuously add and shed discs of the outer segments [19]. This renewal of the outer segment has been suggested to be related to the recovery of the length of the foveal photoreceptor outer segments [19]. The ELM is the first structure to recover after MH closure [25, 27, 29]. The ELM is considered to consist of zonular adherence between photoreceptor inner segment and the Müller cell processes, and there is no zonula occludens in ELM [32]. Thus, ELM is macromolecule-impermeant intermediate junction, and microscopic particles such as horseradish peroxidase can pass through the intercellular space of ELM. ELM is thought to have a supportive function in maintaining the alignment and orientation of the photoreceptor [33]. Therefore, restoration of the ELM may be necessary for sequential photoreceptor outer segment repair, although the reason why the structure of ELM is most preserved in various retinal disease remains unclear. A continuous ELM has been considered to be a sign of intact photoreceptor cell bodies and the Müller cells, and the IS/OS junction or COST rarely recovered without a recovery of the ELM [25–27, 29]. Reconstruction of the foveal ELM line in the early postoperative period can help to predict subsequent restoration of the foveal photoreceptor layer and the potential for better visual outcomes after MH surgery [29]. Bottoni et al. [27] reported that an intact outer nuclear layer at the fovea also seems to be necessary to achieve a complete restoration of the photoreceptor microstructure.

4. Histology and Optical Coherence Tomographic Image

Among three highly reflective lines depicted inside the RPE on the SD-OCT image, the ELM is considered to consist of zonular adherence between photoreceptor inner segment and the Müller cell processes [32]. The ELM line typically is thinner and much fainter than the other two lines. The second line has been commonly ascribed to the boundary between the inner segments and outer segments of the photoreceptors (IS/OS) [3]. The COST line, also known as the Verhoeff membrane [16], is considered to be attributed to scattering from the tips of the cone outer segment, which is shorter than the rod outer segment, in the region of interdigitation between the photoreceptor outer segment and the RPE cell processes that extend into the outer segment layer.

Most recently, Spaide and Curcio [3] evaluated the validity of commonly used anatomical designations for these hyperreflective lines. A scale model of outer retinal morphology was created using published information for direct comparison with SD-OCT scans. Their analysis showed a high likelihood that the SD-OCT lines attributed to the ELM (the first, innermost line) are correctly attributed. Comparative analysis showed that the second line, often attributed to the boundary between inner and outer segments of the photoreceptors, actually aligns with the ellipsoid portion of the inner segments. The third line corresponded to an ensheathment of the cone outer segments by apical processes of the RPE in a structure known as the contact cylinder.

Further studies regarding comparison between OCT images *in vivo* with histological correlative will be needed to understand what the change of OCT finding actually means. Only by making an accurate assessment of OCT findings, we can understand the precise changes of the photoreceptor *in vivo* in various retinal diseases.

5. Conclusion

Three highly reflective lines in the outer retina, which are the ELM, IS/OS and COST, can serve as hallmarks for the evaluation of photoreceptor condition. In RP patients, the ELM, IS/OS, and COST lines are shortened with

the progression of the disease. The shortening of the ELM, IS/OS, and COST lines is significantly associated with each other. In each eye, the line length was longest in the ELM, followed by the IS/OS, and COST, suggesting that retinal layer becomes disorganized first at the COST line, followed by the IS/OS line and finally the ELM line [9]. On the other hand, retinal layer becomes restored first at the ELM, followed by the IS/OS and finally the COST after MH surgery. Taken together, there may be a directionality of the photoreceptor impairment or restoration on OCT image. Further studies with the use of high-resolution images of OCT should lead to understanding a more precise process of the photoreceptor impairment or restoration in various retinal diseases.

Conflict of Interest

The authors have no proprietary interests in any aspect of this paper.

Acknowledgments

This work was supported in part by Grant-in Aid 22591929 (to Y. Mitamura) from the Ministry of Education, Science, Sports and Culture, Japan.

References

[1] Y. Mitamura, S. Mitamura-Aizawa, T. Nagasawa, T. Katome, H. Eguchi, and T. Naito, "Diagnostic imaging in patients with retinitis pigmentosa," *Journal of Medical Investigation*, vol. 59, no. 1-2, pp. 1–11, 2012.

[2] D. F. Kiernan, W. F. Mieler, and S. M. Hariprasad, "Spectral-domain optical coherence tomography: a comparison of modern high-resolution retinal imaging systems," *American Journal of Ophthalmology*, vol. 149, no. 1, pp. 18–31, 2010.

[3] R. F. Spaide and C. A. Curcio, "Anatomical correlates to the bands seen in the outer retina by optical coherence tomography: literature review and model," *Retina*, vol. 31, no. 8, pp. 1609–1619, 2011.

[4] Y. Mitamura, K. Hirano, T. Baba, and S. Yamamoto, "Correlation of visual recovery with presence of photoreceptor inner/outer segment junction in optical coherence images after epiretinal membrane surgery," *British Journal of Ophthalmology*, vol. 93, no. 2, pp. 171–175, 2009.

[5] A. Hagiwara, S. Yamamoto, K. Ogata et al., "Macular abnormalities in patients with retinitis pigmentosa: prevalence on OCT examination and outcomes of vitreoretinal surgery," *Acta Ophthalmologica*, vol. 89, no. 2, pp. e122–e125, 2011.

[6] S. Aizawa, Y. Mitamura, T. Baba, A. Hagiwara, K. Ogata, and S. Yamamoto, "Correlation between visual function and photoreceptor inner/outer segment junction in patients with retinitis pigmentosa," *Eye*, vol. 23, no. 2, pp. 304–308, 2009.

[7] Y. Mitamura, S. Aizawa, T. Baba, A. Hagiwara, and S. Yamamoto, "Correlation between retinal sensitivity and photoreceptor inner/outer segment junction in patients with retinitis pigmentosa," *British Journal of Ophthalmology*, vol. 93, no. 1, pp. 126–127, 2009.

[8] S. Aizawa, Y. Mitamura, A. Hagiwara, T. Sugawara, and S. Yamamoto, "Changes of fundus autofluorescence, photoreceptor inner and outer segment junction line, and visual function in patients with retinitis pigmentosa," *Clinical and Experimental Ophthalmology*, vol. 38, no. 6, pp. 597–604, 2010.

[9] A. Hagiwara, Y. Mitamura, K. Kumagai, T. Baba, and S. Yamamoto S, "Photoreceptor impairment on optical coherence tomographic images in patients with retinitis pigmentosa," *British Journal of Ophthalmology*, vol. 97, no. 2, pp. 237–238, 2013.

[10] T. Wakabayashi, M. Sawa, F. Gomi, and M. Tsujikawa, "Correlation of fundus autofluorescence with photoreceptor morphology and functional changes in eyes with retinitis pigmentosa," *Acta Ophthalmologica*, vol. 88, no. 5, pp. e177–e183, 2010.

[11] A. H. Milam, Z. Y. Li, and R. N. Fariss, "Histopathology of the human retina in retinitis pigmentosa," *Progress in Retinal and Eye Research*, vol. 17, no. 2, pp. 175–205, 1998.

[12] S. D. Barrong, M. H. Chaitin, S. J. Fliesler, D. E. Possin, S. G. Jacobson, and A. H. Milam, "Ultrastructure of connecting cilia in different forms of retinitis pigmentosa," *Archives of Ophthalmology*, vol. 110, no. 5, pp. 706–710, 1992.

[13] E. L. Berson and M. Adamian, "Ultrastructural findings in an autopsy eye from a patient with Usher's syndrome type II," *American Journal of Ophthalmology*, vol. 114, no. 6, pp. 748–757, 1992.

[14] A. H. Milam, Z. Y. Li, A. V. Cideciyan, and S. G. Jacobson, "Clinicopathologic effects of the Q64ter rhodopsin mutation in retinitis pigmentosa," *Investigative Ophthalmology and Visual Science*, vol. 37, no. 5, pp. 753–765, 1996.

[15] K. Tsunoda, K. Fujinami, and Y. Miyake Y, "Selective abnormality of cone outer segment tip line in acute zonal occult outer retinopathy as observed by spectral-domain optical coherence tomography," *Archives of Ophthalmology*, vol. 129, no. 8, pp. 1099–1101, 2011.

[16] V. J. Srinivasan, B. K. Monson, M. Wojtkowski et al., "Characterization of outer retinal morphology with high-speed, ultrahigh-resolution optical coherence tomography," *Investigative Ophthalmology and Visual Science*, vol. 49, no. 4, pp. 1571–1579, 2008.

[17] M. A. Lazow, D. C. Hood, R. Ramachandran et al., "Transition zones between healthy and diseased retina in choroideremia (CHM) and Stargardt disease (STGD) as compared to retinitis pigmentosa (RP)," *Investigative Ophthalmology and Visual Science*, vol. 52, no. 13, pp. 9581–9590, 2011.

[18] T. Wakabayashi, Y. Oshima, H. Fujimoto et al., "Foveal microstructure and visual acuity after retinal detachment repair: imaging analysis by Fourier-domain optical coherence tomography," *Ophthalmology*, vol. 116, no. 3, pp. 519–528, 2009.

[19] C. J. Guérin, G. P. Lewis, S. K. Fisher, and D. H. Anderson, "Recovery of photoreceptor outer segment length and analysis of membrane assembly rates in regenerating primate photoreceptor outer segments," *Investigative Ophthalmology and Visual Science*, vol. 34, no. 1, pp. 175–183, 1993.

[20] T. Sakai, J. B. Calderone, G. P. Lewis, K. A. Linberg, S. K. Fisher, and G. H. Jacobs, "Cone photoreceptor recovery after experimental detachment and reattachment: an immunocytochemical, morphological, and electrophysiological study," *Investigative Ophthalmology and Visual Science*, vol. 44, no. 1, pp. 416–425, 2003.

[21] B. Cook, G. P. Lewis, S. K. Fisher, and R. Adler, "Apoptotic photoreceptor degeneration in experimental retinal detachment," *Investigative Ophthalmology and Visual Science*, vol. 36, no. 6, pp. 990–996, 1995.

[22] C. C. Barr, "The histopathology of successful retinal reattachment," *Retina*, vol. 10, no. 3, pp. 189–194, 1990.

[23] M. Shimozono, A. Oishi, M. Hata et al., "The significance of cone outer segment tips as a prognostic factor in epiretinal membrane surgery," *American Journal of Ophthalmology*, vol. 153, no. 4, pp. 698–704, 2012.

[24] A. Oishi, M. Hata, M. Shimozono, M. Mandai, A. Nishida, and Y. Kurimoto, "The significance of external limiting membrane status for visual acuity in age-related macular degeneration," *American Journal of Ophthalmology*, vol. 150, no. 1, pp. 27–32, 2010.

[25] E. Ooka, Y. Mitamura, T. Baba, M. Kitahashi, T. Oshitari, and S. Yamamoto, "Foveal microstructure on spectral-domain optical coherence tomographic images and visual function after macular hole surgery," *American Journal of Ophthalmology*, vol. 152, no. 2, pp. 283–290, 2011.

[26] Y. Itoh, M. Inoue, T. Rii, T. Hiraoka, and A. Hirakata, "Correlation between length of foveal cone outer segment tips line defect and visual acuity after macular hole closure," *Ophthalmology*, vol. 119, no. 7, pp. 1438–1446, 2012.

[27] F. Bottoni, S. De Angelis, S. Luccarelli, M. Cigada, and G. Staurenghi, "The dynamic healing process of idiopathic macular holes after surgical repair: a spectral-domain optical coherence tomography study," *Investigative Ophthalmology and Visual Science*, vol. 52, no. 7, pp. 4439–4446, 2011.

[28] T. Baba, S. Yamamoto, M. Arai et al., "Correlation of visual recovery and presence of photoreceptor inner/outer segment junction in optical coherence images after successful macular hole repair," *Retina*, vol. 28, no. 3, pp. 453–458, 2008.

[29] T. Wakabayashi, M. Fujiwara, H. Sakaguchi, S. Kusaka, and Y. Oshima, "Foveal microstructure and visual acuity in surgically closed macular holes: spectral-domain optical coherence tomographic analysis," *Ophthalmology*, vol. 117, no. 9, pp. 1815–1824, 2010.

[30] Y. Itoh, M. Inoue, T. Rii, T. Hiraoka, and A. Hirakata, "Significant correlation between visual acuity and recovery of foveal cone microstructures after macular hole surgery," *American Journal of Ophthalmology*, vol. 153, no. 1, pp. 111–119, 2012.

[31] D. H. Anderson, C. J. Guérin, P. A. Erickson, W. H. Stern, and S. K. Fisher, "Morphological recovery in the reattached retina," *Investigative Ophthalmology and Visual Science*, vol. 27, no. 2, pp. 168–183, 1986.

[32] M. Gloesmann, B. Hermann, C. Schubert, H. Sattmann, P. K. Ahnelt, and W. Drexler, "Histologic correlation of pig retina radial stratification with ultrahigh-resolution optical coherence tomography," *Investigative Ophthalmology and Visual Science*, vol. 44, no. 4, pp. 1696–1703, 2003.

[33] D. M. Albert and J. W. Miller, *Principles and Practice of Ophthalmology*, Saunders Elsevier, Philadelphia, Pa, USA, 3rd edition, 2008.

Hindawi Publishing Corporation
Journal of Ophthalmology
Volume 2013, Article ID 687165, 6 pages
http://dx.doi.org/10.1155/2013/687165

Clinical Study

Diurnal Choroidal Thickness Changes in Normal Eyes of Turkish People Measured by Spectral Domain Optical Coherence Tomography

Ozen Ayrancı Osmanbasoglu,[1] Zeynep Alkin,[1] Abdullah Ozkaya,[1] Yavuz Ozpınar,[1] Ahmet Taylan Yazici,[1] and Ahmet Demirok[1,2]

[1] *Beyoglu Eye Training and Research Hospital, Retina Clinic, Istanbul 34421, Turkey*
[2] *Istanbul Medeniyet Unıversity, Istanbul, Turkey*

Correspondence should be addressed to Ozen Ayrancı Osmanbasoglu; ozayranci@hotmail.com

Received 21 December 2012; Accepted 24 February 2013

Academic Editor: Yoshinori Mitamura

Purpose. To analyse the diurnal variation of central choroidal thickness (CCT) in healthy emetropic patients during working hours. *Methods*. Fifty healthy young emmetrpic volunteers were included in this study. CCT was measured at 9 AM and 4 PM with spectral domain optical coherence tomography (Spectralis, Heidelberg Engineering) with enhanced depth imaging. Diurnal variation of CCT, the correlation between rigth and left eyes and the demographic factors affecting this variation were assessed. *Findings*. The mean CCT at 9 AM and 4 PM was 308.7 ± 64.5 μm and 308.7 ± 62 μm, respectively, with a mean diurnal amplitude of −0.03 ± 14.7 μm, ranging between −55 μm and 47 μm, the difference was statistically insignificant (P: 0.9). There were positive correlations between right and left eyes among CCT measurements at 9 AM, 4 PM and the mean amplitude of diurnal change (r: 0.65, $P < 0.01$; r: 0.60, $P < 0.01$; r: 0.45, P: 0.00, resp.). There was a statistically significant negative correlation between the magnitude of diurnal change and age (r: −0.27, P: 0.01). *Conclusion*. Although the mean CCT in the all group does not show significant variation during working hours, the pattern of diurnal variation may vary from person to person according to age, and there is a great harmony between the two eyes.

1. Introduction

The choroid is the middle vascular layer of the eye, lying between the retina and sclera. It accounts for 85 percent of ocular blood flow and plays a major role in the oxygenation, nourishment, and viability of retinal pigment epithelium and the outer retinal layers, which have the highest metabolic activity. Choroidal changes such as hyperpermeability, vascular insufficiency, thickening, and thinning were shown to play a role in the pathogenesis of chorioretinal disease. With the recent improvements in technology, Spaide et al. [1] developed the enhanced depth imaging (EDI) technique by using spectral-domain optical coherence tomography (OCT), which enables the visualization and measurement of the choroidal layer. Many studies have been published reporting the choroidal thickness (CT) of patients with various retinal disorders such as central serous chorioretinopathy [2–4], age-related macular degeneration [4–8], polypoidal choroidal vasculopathy [7, 8], Vogt-Koyanagi-Harada syndrome [9], and macular hole [10], multiple evanescent white dot syndrome [11] and diabetic retinopathy [12]. Also, the normative data of choroidal thickness of healthy individuals were reported as a guide for further investigations [13–17]. Therefore, OCT is a valuable tool for the diagnosis and management of chorioretinal diseases as well as helping clinicians understand the underlying pathology.

During the followup and management of patients, repeated OCT evaluations have to be done during different working hours on different visits. Due to its high blood flow and poor autoregulation, choroidal thickness variation could

be seen intraindividually. The awareness of circadian changes can lead the management or understanding the mechanism of the diseases. The presence of diurnal fluctuations of human choroidal thickness also has been studied by Usui et al. [18], where the choroidal thickness was measured every two hours during a twenty-four-hour period, but the population was at myopic range. Also Tan and colleagues [19] described the pattern and magnitude of diurnal variation of choroidal thickness of twelve patients whose refractive error ranged between −4.1 and +2.0 s. The purpose of this study is to analyse the diurnal variation of central choroidal thickness in healthy emetropic patients during working hours to determine the affecting factors on diurnal variation in the Turkish population.

2. Materials and Method

2.1. Subjects. This is a prospective, cross-sectional, observational study performed at Beyoğlu Eyoğlu Eye Training and Research Hospital. The study protocol was approved by the local ethics committee, and all of the patients signed an informed consent. The methodology of the study was designed in accordance with the tenets of the Helsinki Declaration.

Fifty healthy volunteers were included in the study. The exclusion criteria included any ocular illnesses such as the presence of macular abnormality, glaucoma, previous ocular surgery or trauma, amblyopia, visual acuity larger than 0,00 logarithm of the Minimum Angle of Resolution (LogMAR) Unit, refractive error (RE) ranging outside −1.00 +1.00 diopters, axial length (AL) outside 22–25 mm, any systemic vascular diseases such as hypertension, diabetes mellitus and inability to cooperate during screening by OCT examination.

2.2. Examination Procedures. All participants underwent a complete ocular examination. All of the procedures were performed once on the same day of OCT examination before the first measurement. Objective refraction was measured by autorefractometer (Canon-RK-F1, serial number: 112213), and best corrected visual acuity was recorded using Snellen charts and converted to LogMAR for analyses. Biomicroscopic and fundoscopic examination with a 90 D lens was performed, and intraocular pressure was measured with a Goldmann applanation tonometer. Ocular axial length was measured using interferometry (IOL-Master, version 918471, model 1322-734; Carl Zeiss Meditec, La Jolla, CA, USA).

OCT scans were performed by the two investigators (either O. A. Osmanbasoglu or Z. Alkin) at 9 AM and 4 PM on an outpatient basis for both eyes. Pupils were dilated with tropicamide 1 percent (Alcon, RØdovre, Denmark) before each OCT examination. Central macular thickness was measured automatically with the software of the system using fast macular examination mode. The choroid was visualized by enhanced depth imaging technique with spectral domain optical coherence tomography (Spectralis OCT, Heidelberg Engineering, Heidelberg, Germany) using a standardised scanning protocol. A single line of 6 mm length centered horizontally on the fovea was used for the visualization of the choroid. To maximise signal-to-noise ratio and reduce speckle noise, the images were acquired in high-resolution protocol. The TruTrack active eye tracking system, which enables the capture of multiple images in the same location, and the automatic real-time (ART) mean function, which combines these images, were used during each image acquisition. ART was set up for 100 frames.The initial (baseline) measurement at 9 AM was set as a reference, and the second scan was done at the same point on the fovea with the eye tracking system.

Choroidal thickness was measured subfoveally using the manual calipers provided by the device software. To avoid interobserver variation, both of the graders measured the choroidal thickness at the same time, and two measurements were taken for each patient in order to assess intrasession variability. Measurement was performed perpendicularly from the outer part of the hyperreflective line (retinal pigment epithelial layer) to the line corresponding to the corneoscleral junction. If the corneoscleral junction could not be identified exactly or the quality of the images was low (below Q 25), the eye was dismissed from the study.

2.3. Outcome Measures. This study evaluated the mean choroidal and central retinal thickness at 9 AM and 4 PM and the diurnal change in choroidal thickness. Demographic factors affecting the diurnal variation were also investigated.

2.4. Statistical Analysis. Statistical analyses were made using commercially available software SPSS version 16.0 (SPSS Inc., Chicago, IL). For the statistical analyses, the mean (SD) of the differences was calculated. The images were measured twice at the same time by the two observers; the difference of the two measurements was analysed with paired sample t test, and intraclass correlation was performed by a Pearson correlation test. Bland-Altman plot was generated to assess agreement of measurements between the two measurements of the same session. Differences in thickness between measurements were plotted against mean choroidal thickness measurements on the graph [20]. A paired sample t-test was used to compare the diurnal change of the central subfoveal choroidal and central macular thickness. The correlation coefficient (Pearson correlation) was calculated for the relationship between the subfoveal choroidal and retinal thicknesses. The magnitude of CT change was calculated by extracting CT value that was measured at 4 PM from the value measured at 9 AM. The relationship between age, axial length and the magnitude of diurnal change was analysed with Pearson correlation. To evaluate the effect of sex on diurnal variation, patients were grouped and the differences between the groups were analysed with a t test. P values of 0.05 were considered statistically significant.

3. Results

One hundred eyes of fifty patients (27 female, 23 male) were evaluated. None of the participants had a history of systemic or ocular disease. The measurements of eighty-five

eyes (43 right eye, 42 left eye) were eligible for analysis, and fifteen eyes were dismissed from the study because of low image quality and/or inadequate evaluation of corneoscleral junction. The mean age was 45.2 ± 7.4 years. All eyes had the best corrected visual acuity of 0,00 LogMAR Unit, and mean refractive error was +0.50 ±0.25 diopters. Mean axial length was 23.1 ± 0.8 mm. Mean intraocular pressure was 15.3 ± 2 mmHg. Table 1 shows demographic data.

The mean baseline choroidal thicknesses among eighty-five eyes at 9 AM and 4 PM were 308.7 ± 64.5 μm, and 308.7 ± 62 μm respectively, with a mean diurnal amplitude of −0.03 ± 14.7 μm; the difference was statistically insignificant (P: 0.9). Of those patients who had two eyes included in the study (n: 35), mean choroidal thickness at 9 AM and 4 PM and the mean diurnal amplitude of the right eyes were 304.9 ± 64 μm, 305.9 ± 59.6 μm, and −0.97 ± 16.6 μm, and the left eyes were 312.5 ± 75.6 μm, 311.6 ± 65 μm and 0.92 ± 12.7 μm, respectively. There were positive correlations between the right and left eyes in the morning and evening choroidal thickness measurements and the mean amplitude of diurnal change (r: 0.65, $P < 0.01$; r: 0.60, $P < 0,01$; r: 0.45, P: 0.00 resp.). Over the same time period, the baseline central macular thickness measurement at 9 AM was 272.2 ± 17 μm, and it did not show significant variation on a paired sample t test (P: 0.6). The morning and evening central macular and choroidal thickness did not show any significant correlation (r: −0.06, P: 0.6; r: −0.03, P: 0.7). Table 2 summarizes baseline and follow-up measurements.

For the baseline and the second OCT analysis, the measurements were repeated twice, and the mean of differences for the measurements of the same eye in the same session was 4.5 ± 14.6 μm (range from −19 to 18 μm), the difference was insignificant on a paired t test (P: 0.7), and the intraclass correlation of these two measurements was statistically significant (r: 0.9, P: 0.00). A Bland-Altman plot of difference against mean choroidal thickness showed no significant change in intrasession variability for the range of choroidal thickness measurements seen in healthy subjects, and the plot is shown in Figure 1. Although the mean diurnal variation in all groups was −0.03 ± 14.7 and the difference was insignificant, the magnitude of change ranged from −55 μm to 47 μm; therefore, some of the patients showed diurnal variation, and as such six remained unchanged (mean of change was 0.00 μm), forty showed a decrease of mean 11.2 (9.5) μm, and thirty-nine showed an increase of mean 11.5 (11.07) μm.

The eyes were grouped into two subgroups according to the sex for the purpose of additional subanalyses. The CT thickness and the diurnal magnitude were analysed. The mean CT at 9 AM and 4 PM and the magnitude of change of female patients (mean AL: 22.9 mm) were 327.5 (53.8) μm, 320.1 (52.1) μm, and 2.4 (14.5) μm; male patients (mean AL: 23.5 mm) were 293.1 ± 72.2 μm, 295.9 ± 70 μm, and −2.8 ± 14.8 μm, respectively. The mean CT at 9 AM and 4 PM was statistically insignificant between groups when measurements were adjusted according to the AL (P: 0.7, P: 0.6 resp.), and the magnitude of diurnal change was insignificant in both groups (P: 0.3, P: 0.2 resp.).

There was a weak but statistically significant negative correlation between the magnitude of diurnal change and age (r: −0.27, P: 0.01). For additional analyses, the eyes were grouped according to age as Group 1 (30–39 years, n: 19), Group 2 (40–49 years, n: 41), and Group 3 (50–57 years, n: 25). The magnitude of change was +7.1 (11.8), −0.3 (15.7), and −4.7 (13.4), respectively and shown in Figure 2. The diurnal variation in Group 1 and Group 3 was significant (P: 0.02, P: 0.03) while it was insignificant (P: 0.7) in Group 2 with a paired t-test. There was a statistically significant difference between groups regarding the diurnal variation with Kruskal-Wallis test (P: 0.00). The correlation between axial length and diurnal variation was insignificant with Pearson correlation (r: −0.19; P: 0.3).

Table 1: Demographics of the subjects in the study.

Parameters	Mean (SD)	Range
Age, y	45.2 (7.4)	30–57
Axial length, mm	23.1 (0.8)	21.3–24.9
Refractive error, D	+0.50 ± 0.25	−1.00 to +0.75
IOP, mmHg	15.3 ± 1.9	8–19

SD: standard deviation.

Table 2: Choroidal thickness in all groups, RE and LE and central macular thickness at 9 AM, 4 PM, and the magnitude of diurnal change.

	At 9 AM Mean (SD) (range)	At 4 PM Mean (SD) (range)	Diurnal change Mean (SD) (range)	P
All eyes, CT, μm	308.7 (64.5) (145–496)	308.7 (62) (140–485)	−0.03 (14.7) (−55 to 47)	0.9
All eyes, CMT, μm	271.1 (18.1) (243–328)	271.3 (17) (244–329)	−0.17 (3.02) (−8 to 8)	0.6
RE CT, μm	304.9 (64) (152–444)	305.9 (59) (150–423)	−0.97 (16.6) (−55 to 47)	0.9
LE CT, μm	312.5 (65.4) (145–496)	311.6 (65) (140–485)	0.92 (12.7) (−36 to 36)	0.9

CT: choroidal thickness, CMT: central macular thickness, RE: right eye, LE: left eye.

4. Discussion

In this study we measured the choroidal thickness twice a day, during working hours (early in the morning and late in the afternoon), using EDI spectral domain OCT in the healthy emetropic Turkish population, to investigate diurnal variation. In a study by Ikuno et al. [14], two out of eighty-six eyes were excluded due to poor image quality because of poor fixation by 1060 nm HP-OCT, which is based on swept-source OCT technology. Chen et al. [21] reported that one subject was excluded because of a poor-quality scan due to poor fixation by EDI spectral domain OCT. Manjunath et al. [17] reported that in one of four eyes, the corneoscleral boundary was unclear with Cirrus HD-OCT due to a suboptimal number of averaged OCT B scans, the lack of eye tracking software, and the potential for eye movement

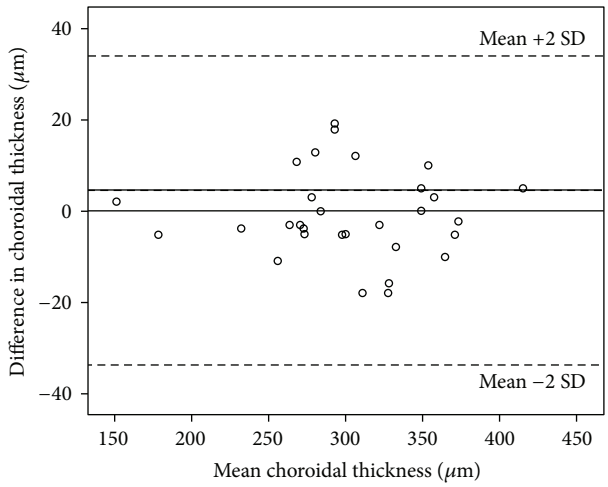

Figure 1: Bland-Altman plot for choroidal thickness. Dotted lines delinate mean and %95 confidence limits of agreement.

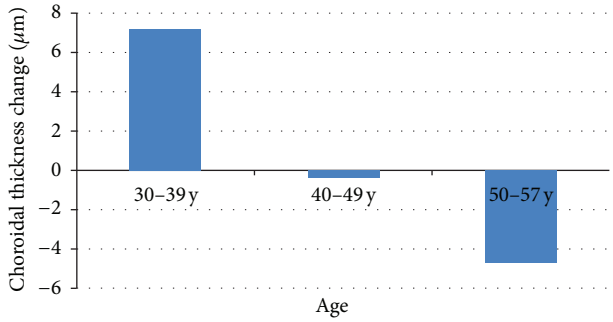

Figure 2: The magnitude of diurnal change according to age group.

during imaging. Our results were comparable with previous studies that, in spite of using high-resolution protocol, an eye tracking system, and ART function, due to inadequate fixation or densely pigmented retinal pigment epithelium, the corneoscleral junction was identified clearly only in 85 percent of eyes for both measurements, and both eyes of the same patient were included in 70 percent of patients in our study. Although swept-source OCT can obtain high-quality images over a greater imaging depth as compared with SD-OCT, corneoscleral junction can be identified with both machines. But due to the poor fixation or densely pigmented retina pigment epithelium, the corneoscleral junction could not be assessed adequately with both of the devices. Ikuno et al. [14] used swept-source OCT and reported exclusion of 2 eyes because of this reason. But in the study of Usui et al. [18], they did not report such a ratio. Besides, the eye tracking system of Heidelberg spectral domain OCT enables us to measure the exact same location over the fovea. Since the choroid does not have an uniform structure for the assessment of diurnal variation, the exact same location had to be remeasured for the accurate results. This is the superiority of SD-OCT over swept-source OCT and the advantage of this study.

The mean choroidal thickness in our study was 308.7 μm, ranging between 140 μm and 496 μm. In a study by Usui et al. [18], the mean CT was 280.3 μm measured by HP-OCT (Topcon), but the population was younger and more myopic. Tan et al. [19] reported a mean CT of 372.2 μm measured by SD-OCT in a younger age group, but the RE was similar. Toyokawa et al. [22] reported a mean CT of 308.5 μm, similar to our study, but the mean age was older (62.6 years). In the study by Ikuno et al. [14], the mean choroidal thickness was 354 μm by 1060 nm HP-OCT, the patients had a wider range of age (23–88 years old), and the mean RE was −1.9 ± 2.3 D. Our results were higher than the 287 ± 76 μm measured with Heidelberg SD-OCT in a study of thirty-four healthy American subjects that was reported Margolis and Spaide [13]. Li and colleagues [15] reported a mean subfoveal choroidal thickness in ninety-three Danish university students measured by Heidelberg SD-OCT at 342± 118 μm, in a younger age group (24.9 years old) whose RE was −1.43 D. It has been reported that CT varies according to age and AL. In previous studies by Margolis and Spaide [13] and Ikuno et al., [14], there were decreases of 15 μm and 14 μm in CT, respectively, for every 10 years. Also it has been reported that choroidal thickness changes −58.2 [15] to −22.4 [1] for every increment in 1 mm of AL. Therefore, the differences in mean choroidal thickness between the studies may result from differences in the study population, OCT machine used, and measuring software.

To the best of our knowledge, this is the largest study of diurnal variations in healthy emetropic patients. We did not observe a significant average diurnal variation in choroidal thickness in our study population. Previous investigators demonstrated significant diurnal variations in CT. Brown et al. [23] used the signal processing technique and found a mean CT of 426 μm and a diurnal change of 59.5 ± 24 μm. Chakraborty and colleagues [24] also used the signal processing technique and reported the findings of diurnal variations in thirty healthy eyes. They showed that choroidal thickness increases progressively from 12 PM to 6 PM and the mean amplitude of thickness change was 29 ± 16 μm. Usui et al. [18] reported a significant subfoveal choroidal thickness circadian change by using a high penetration OCT (Topcon). The magnitude of change averaged 33 μm in the thirty-eight eyes of nineteen healthy subjects (mean age was 34.8 years), with the thickest at 3 AM and thinnest at 6 PM. However, unlike our study, most of the subjects were at myopic range with a mean RE of −4.4 ± 2.4; the population was younger and the mean baseline CT was thinner than ours. Tan et al. [19] also reported a significant diurnal variation in twelve healthy volunteers (mean age was 30 years and mean RE was −0.46 ± 1.3 D) measured by Heidelberg SD-OCT and averaging 33.3 μm, with the thickest being at 9 AM and the thinnest at 5 PM, which is comparable to the findings of Usui et al. [18]. However, the study population is younger than ours and the mean baseline CT is thicker. Toyokawa et al. [22] reported a significant diurnal variation of 20 μm, with the thickest being in the evening, although the baseline choroidal thickness is the same and the study population was older than ours. In studies by Usui et al. [18] and Tan et al. [19], the mean choroidal thickness decreased during day while Chakraborty et al. [24] and Toyokawa et al.'s [22] population showed an increase. Although these studies used different measurement

techniques that consisted of optical biometers and OCT and there were differences in demographic data between groups, they both showed a significant diurnal variation, averaging from 59.5 μm to 33 μm. Although the mean CT difference decreased during the day, six out of thirty-eight eyes in Usui et al.'s [18] study showed an increment and thirty-two showed a decrement from the baseline. The magnitude of diurnal change ranged from −55 μm to 47 μm in this study. Some patients showed an increment, some stayed stable, and others showed a decrement from the baseline, but the average was statistically insignificant. Demographic differences such as age and AL, the differences in the baseline central subfoveal choroidal thickness, and the diversity of OCT machines used in our study and in previous studies [18, 19, 22] may lead to the differences in the study results. On the other hand, Tan et al. [19] also demonstrated that there is a remarkable congruence in the diurnal pattern of individual eyes on different days. However, this and the previous studies [18, 19, 21] showed a significant correlation between the right and left eyes among CT at 9 AM and 4 PM and the magnitude of diurnal change. Therefore, the exact pattern of diurnal variation may vary from person to person and may not be constant in all individuals, but there is harmony between two eyes. In this series, the central macular thickness measurement did not show any variation between two measurement points. This finding is consistent with previous reports [18, 19]. Also there was no correlation between the central macular and choroidal thicknesses.

In previous reports by Li et al. [15], the subfoveal choroid was thicker in men than women and there was a 62 μm difference between groups. We did not find any differences among CT and CT variation in between the two sexes when we adjust the two groups according to AL. To the best of our knowledge, this is the only study analysing diurnal variations in between two sexes.

Previous studies have reported similar negative correlations between choroidal thicknesses with age [13, 16, 17]. Although the diurnal variation of CT was insignificant in all groups in this study, we found differences between decades. In young patients, choroidal thickness tends to increase during the day while the diurnal variation becomes negatively correlated with the age increments. This finding is also comparable with the study by Tan et al. [19], but the older population in the study by Toyokawa et al. [22] showed a significant increase in CT diurnally.

Previous studies reported diurnal variations in AL [16, 19, 24]. We measured AL once in the morning, and we did not analyse AL change in this study. Therefore, the relationship between CT change and AL was made with baseline AL measurements. We did not find any correlation between AL and CT change, which contradicts a study by Tan et al. [19]. Although mean AL values did not differ much in these two studies, it had a narrower interval in our study, which may cause such a discrepancy between the studies.

The main limitations of this study are that systemic factors such as diastolic and systolic blood pressure were not assessed, diurnal IOP and AL change were not analysed, and only healthy emetropic patients with a limited range of age were included. Also the choroidal thickness was assessed during two time points only in working hours and in only one day so the variation during evening and night and the variation on different days were not assessed in this study.

In conclusion, the pattern of diurnal variation of choroidal thickness may remain stable and may show a decrease or increase from the baseline according to age, but there is great harmony between the two eyes. Therefore, when assessing choroidal thickness in the clinic, a patient's individual diurnal variation pattern should be taken into account.

Conflict of Interests

The authors declare that there is no conflict of interests.

Disclosure

This study was not presented in any meeting. None of the authors has a financial or proprietary interest in a product, method, or the material used in the study.

References

[1] R. F. Spaide, H. Koizumi, and M. C. Pozonni, "Enhanced depth imaging spectral-domain optical coherence tomography," *American Journal of Ophthalmology*, vol. 146, no. 4, pp. 496–500, 2008.

[2] Y. Imamura, T. Fujiwara, R. Margolis, and R. F. Spaide, "Enhanced depth imaging optical coherence tomography of the choroid in central serous chorioretinopathy," *Retina*, vol. 29, no. 10, pp. 1469–1473, 2009.

[3] Y. T. Kim, S. W. Kang, and K. H. Bai, "Choroidal thickness in both eyes of patients with unilaterally active central serous chorioretinopathy," *Eye*, vol. 25, pp. 1635–1640, 2011.

[4] S. W. Kim, J. Oh, S. S. Kwon, J. Yoo, and K. Huh, "Comparison of choroidal thickness among patients with healthy eyes, early age-related maculopathy, neaovascular age-related macular degeneration, central serous chorioretinopathy and polypoidal choroidal vasculopathy," *Retina*, vol. 31, pp. 1904–1911, 2011.

[5] A. Wood, A. Binns, T. Margrain et al., "Retinal and choroidal thickness in early age-related macular degeneration," *American Journal of Ophthalmology*, vol. 152, pp. 1030–1038, 2011.

[6] A. A. Ellabban, A. Tsujikawa, K. Ogino et al., "Choroidal thickness after intravitreal ranibizumab injections for choroidal neovascularization," *Clinical Ophthalmology*, vol. 6, pp. 837–844, 2012.

[7] H. Koizumi, T. Yamagishi, T. Yamazaki et al., "Subfoveal choroidal thickness in typical age-related macular degeneration and polypoidal choroidal vasculopathy," *Graefe's Archive for Clinical and Experimental Ophthalmology*, vol. 249, pp. 1123–1128, 2011.

[8] S. E. Chung, S. W. Kang, J. H. Lee, and Y. T. Kim, "Choroidal thickness in polypoidal choroidal vasculopathy and exudative age-related macular degeneration," *Ophthalmology*, vol. 118, no. 5, pp. 840–845, 2011.

[9] A. H. C. Fong, K. K. W. Li, and D. Wong, "Choroidal evaluation using enhanced depth imaging spectral-domain optical coherence tomography in Vogt-Koyanagi-Harada disease," *Retina*, vol. 31, no. 3, pp. 502–509, 2011.

[10] K. B. Schaal, S. Pollithy, and S. Dithmar, "Ischoroidal thickness of importance in idiopathic macular hole?" *Ophthalmologe*, vol. 109, pp. 364–368, 2012.

[11] R. Aoyagi, T. Hayashi, A. Masai et al., "Subfoveal choroidal thickness in multiple evanescent white dot syndrome," *Clinical and Experimental Optometry*, vol. 95, pp. 212–217, 2012.

[12] M. Esmaeelpour, B. Povazay, B. Hermann et al., "Mapping choroidal thickness and retinal thickness variation in type 2 diabetes using three-dimensional 1060-nm optical chorence tomography," *Investigative Ophthalmology & Visual Science*, vol. 52, pp. 5311–5316, 2011.

[13] R. Margolis and R. F. Spaide, "A pilot study of enhanced depth imaging optical coherence tomography of the choroids in normal eyes," *American Journal of Ophthalmology*, vol. 147, no. 5, pp. 811–815, 2009.

[14] Y. Ikuno, K. Kawaguchi, T. Nouchi, and Y. Yasuno, "Choroidal thickness in healthy Japanese Subjects," *Investigative Ophthalmology & Visual Science*, vol. 51, pp. 2173–2176, 2010.

[15] X. Q. Li, M. Larsen, and I. C. Munch, "Subfoveal choroidal thickness in relation to sex and axial length in 93 Danish University Students," *Investigative Ophthalmology & Visual Science*, vol. 52, pp. 8438–8441, 2011.

[16] D. Goldenberg, E. Moisseiev, M. Goldstein et al., "Enhanced depth imaging optical coherence tomography: choroidal thickness and correlations with age, refractive error, and axial length," *Ophthalmic Surg Lasers Imaging*, vol. 43, pp. 296–301, 2012.

[17] V. Manjunath, M. Taha, J. G. Fujimoto, and J. S. Duker, "Choroidal thickness in normal eyes measured using cirrus HD optical coherence tomography," *American Journal of Ophthalmology*, vol. 150, no. 3, pp. 325–e1, 2010.

[18] S. Usui, Y. Ikuno, M. Akiba et al., "Circadian changes in subfoveal choroidal thickness and the relationship with circulatory factors in healthy subjects," *Investigative Ophthalmology & Visual Science*, vol. 53, pp. 2300–2307, 2012.

[19] C. S. Tan, Y. Quyang, H. Ruiz, and S. R. Sadda, "Diurnal variation of choroidal thickness in normal healthy subjects measured by spectral domain optical coherence tomography," *Investigative Ophthalmology & Visual Science*, vol. 53, pp. 261–266, 2012.

[20] J. M. Bland and D. G. Altman, "Statistical methods for assessing agreement between two methods of clinical measurement," *Lancet*, vol. 1, no. 8476, pp. 307–310, 1986.

[21] F. K. Chen, J. Yeoh, W. Rahman, P. J. Patel, A. Tufail, and L. Da Cruz, "Topographic variation and interocular symmetry of macular choroidal thickness using enhanced depth imaging optical coherence tomography," *Investigative Ophthalmology & Visual Science*, vol. 53, pp. 975–985, 2012.

[22] N. Toyokawa, H. Kimura, A. Fukomoto, and S. Kuroda, "Difference in morning and evening choroidal thickness in Japanese subjects with no chorioretinal disease," *Ophthalmic Surgery, Lasers & Imaging*, vol. 43, pp. 109–114, 2012.

[23] J. S. Brown, D. I. Flitcroft, G. S. Ying et al., "In vivo human choroidal thickness measurements: evidence for diurnal fluctuations," *Investigative Ophthalmology and Visual Science*, vol. 50, no. 1, pp. 5–12, 2009.

[24] R. Chakraborty, S. A. Read, and M. J. Collins, "Diurnal variations in axial length, choroidal thickness, intraocular pressure and ocular biometrics," *Investigative Ophthalmology & Visual Science*, vol. 52, pp. 5121–5129, 2011.